1 Introduction

Being born at the end of the last century, it's difficult for me to fully appreciate just how dramatic – and how recent – the progress in our understanding of the Universe has been. For millennia, civilizations devised myths to explain the origins of the cosmos and its fate. Today, however, we possess a well-tested theoretical framework that describes the evolution of the Universe from about one second after the Big Bang to the present day and beyond. Known as the standard model of cosmology, or the ΛCDM model, this framework is rooted in Einstein's theory of general relativity and has been refined through a series of paradigm shifts, some of the most consequential occurring only in the past few decades.

Much like the Standard Model of particle physics, ΛCDM is powerful precisely because it explains a vast range of observations using only a small number of parameters. It has withstood numerous experimental tests and challenges. While it is not the final word – offering limited insight into the true nature of dark matter, dark energy, or the physics of inflation – it remains the most robust and predictive model for describing the large-scale evolution of the Universe.

ΛCDM provides the backbone: a model of the Universe on the largest scales. On top of this framework, however, lies the rich tapestry of structure formation: the growth of stars, galaxies, and black holes. Research in physical cosmology today is often split along two broad directions. On one side is the pursuit of ever more precise tests of the ΛCDM model, a field now driven by percent-level measurements that seek signs of new physics in the smallest deviations from theoretical predictions. This often relies on observations of the largest cosmic scales, where the imprint of complex astrophysical processes is negligible or can be marginalized effectively. On the other side lies the study of those very astrophysical processes – nonlinear, chaotic, and often poorly understood. This is not a percent-level science, but an order-of-magnitude one. Yet, it is precisely this limited understanding of galaxy evolution that has made the field ripe for discovery, and indeed, some of the most transformative progress in recent years has come from this domain.

A crucial driver of this recent progress has been the advent of new observatories capable of probing ever earlier cosmic times. By pushing the limits of our observations to higher redshifts[1], these instruments are extending the frontiers of our knowledge and opening up new regimes for discovery. The most prominent recent example is the James Webb Space

[1] The cosmological redshift, z, is a measure of cosmic time: higher redshifts correspond to earlier times in the history of the Universe.

Telescope (JWST), launched in 2021. With its unprecedented sensitivity and resolution, JWST is already reshaping our understanding of the early Universe by revealing surprising properties of the first galaxies and black holes and challenging established theoretical models. It has been an instructive experience to witness this chaotic yet inspiring transformative process taking place during my Ph.D. – progress that also shapes the core of this thesis.

Among the most important findings in the context of galaxy formation is the central role played by supermassive black holes (SMBHs). Initially proposed in the 1960s to explain the immense energy output of quasars, SMBHs quickly became a cornerstone of active galactic nuclei (AGN) theory. By the 1990s, high-resolution observations showed that SMBHs are ubiquitous in the Universe, inhabiting all massive galaxies even in the absence of AGN activity. Tight empirical correlations were discovered between the mass of SMBHs and several properties of the host galaxies, suggesting a scenario of coevolution, or, at the very least, a deep physical connection between black hole growth and galaxy evolution. More recently, the detection of luminous quasars at redshifts beyond $z > 6$ has shown that billion-solar-mass black holes were already in place less than a billion years after the Big Bang, posing significant challenges to our understanding of early black hole growth.

This thesis explores these themes – among others – through a focused investigation of SMBHs as traced by the properties of quasars, particularly in the high-redshift Universe where the earliest stages of SMBH and quasar evolution unfold. Chapters 2–5 are dedicated to this topic. The central idea driving these chapters is that the ΛCDM model provides a robust cosmological framework for describing the large-scale structure and its evolution across cosmic time. By building upon this foundation, we can construct models to understand how SMBHs and quasars form, grow, and evolve, and connect them to observations across a range of redshifts. The overarching goal is to determine how complex astrophysical processes – such as black hole accretion and quasar activity – can be consistently embedded within the standard cosmological paradigm, using a phenomenologically driven approach that bridges theory and data.

Chapters 6 and 7 focus on distinct research directions that fall outside the main scope of this thesis but reflect other projects I pursued before and during my Ph.D., in collaboration with researchers from other subfields. Chapter 6 shifts attention to the opposite end of the black hole mass spectrum: stellar-mass black holes, whose mergers have been detected by gravitational wave observatories such as LIGO, Virgo, and KAGRA. This chapter presents a first step toward addressing a key challenge for the next generation of gravitational wave detectors – expected to operate in the 2030s – which will be so sensitive that overlapping signals in the time domain may complicate the inference of source parameters. Our work quantifies and assesses the impact of this overlap on parameter estimation.

Chapter 7 explores a different class of astrophysical discs – not those around SMBHs, but the protoplanetary discs surrounding young stars, which are the birthplaces of planetary systems. These structures have been extensively studied with the Atacama Large Millimeter/submillimeter Array (ALMA), which provides high-resolution observations in the far infrared. In this chapter, we use ALMA data to infer the vertical structure of protoplanetary discs, shedding light on the early stages of planet formation.

While this introduction focuses primarily on supermassive black holes and extragalactic astrophysics, a complete overview of the contents of all chapters is provided in Section 1.5.

Why this title

What links bright quasars in galaxies far, far away to mergers of stellar-mass black holes in the nearby Universe – detected through their gravitational-wave emission – to the protoplanetary discs we observe in our solar neighbourhood? I asked myself this question when searching for a title for this thesis. While many connections can be drawn, one in particular stood out to me: the idea that, in different ways, this thesis revolves around the concept of *bias*.

Chapter 1 opens by discussing how quasars at $z \approx 4$ appear to be among the most biased tracers of structure in the early Universe. There, we are talking about *cosmological bias* – a concept introduced in Sec. 1.1. In this context, bias quantifies how the spatial distribution of certain astrophysical objects, like quasars, relates to the underlying distribution of dark matter. Because they tend to reside in massive structures, quasars are more clustered than the matter field as a whole, and thus are said to be "biased" tracers of the large-scale distribution of matter. Understanding how different populations of quasars and galaxies trace this distribution is central to embedding black hole and galaxy evolution within a cosmological framework.

Cosmological bias is a somewhat niche but well-defined concept. Later in the thesis, a different kind of bias takes the stage – one that is more familiar to anyone working in data analysis or modeling. Chapter 6 deals with *bias in parameter inference*: how assumptions, modelling choices, and incomplete information can systematically skew the results we extract from data. In this specific case, we assess the bias that can arise from the overlap of multiple gravitational wave signals in the time domain.

Finally, there's a broader, more implicit sense in which bias plays a role: the idea that our window on the Universe is inevitably a biased point of observation. This *observational bias* lies at the core of astronomy as a science. As we show in Chapter 7, however, this bias can also be turned into an advantage. Protoplanetary discs, which are approximately azimuthally symmetric in three dimensions, appear as ellipses on the sky due to projection effects. These same effects distort the apparent shape of substructures – such as the rings and gaps that often characterize discs – breaking their

symmetry in a predictable way that depends on the disc's inclination and intrinsic morphology. As a result, our particular vantage point allows us to constrain the three-dimensional structure of discs, using the bias introduced by projection as a diagnostic tool rather than a limitation.

"From a biased perspective" also reflects my own path through astrophysics. It has been a biased one – shaped by curiosity, but also by chance encounters, guidance from mentors, and the particular set of tools and questions I ended up gravitating towards. There is no single pattern or overarching plan, no carefully laid-out roadmap guiding the journey.

Bias, in its many forms, is something we must acknowledge – whether we aim to model it, correct for it, or simply be aware of it. It shapes what we see, how we interpret it, and what we conclude. But it also reflects who we are: our interests, our choices, our perspective on the Universe. This thesis is one such perspective – a biased one, certainly, but hopefully one worth telling.

1.1 Setting the stage: ΛCDM cosmology and the large-scale structure of our Universe

The ΛCDM model is founded on the "cosmological principle", which posits that, on sufficiently large scales, the Universe is both homogeneous (the same everywhere) and isotropic (the same in all directions). This principle allows a great simplification of Einstein's field equations in general relativity, yielding dynamic solutions that describe a Universe whose overall scale evolves with time, either expanding or contracting according to a scale factor $a(t)$. The corresponding spacetime geometry is captured by the Friedmann-Lemaître-Robertson-Walker (FLRW) metric, which underpins the standard cosmological model. The Friedmann equations relate the dynamics of the scale factor, $a(t)$, to the energy content of the Universe (Friedmann 1922, 1924).

Observational support for this framework came with Edwin Hubble's discovery that distant galaxies exhibit a systematic redshift, indicating that the Universe is indeed expanding (Hubble 1929). This interpretation was further reinforced by Georges Lemaître, who proposed that such expansion implies a finite age and a primordial, hot, and dense origin – a concept that would later be termed the "Big Bang" (Lemaître 1931). In the context of modern cosmology, this singular beginning marks the onset of cosmic time and the starting point for the formation and evolution of all known structures in the Universe.

A cornerstone of the ΛCDM model is the realization that the energy content of the Universe is not composed solely of ordinary (baryonic) matter. Rather, baryons account for only $\approx 5\%$ of the total energy density of

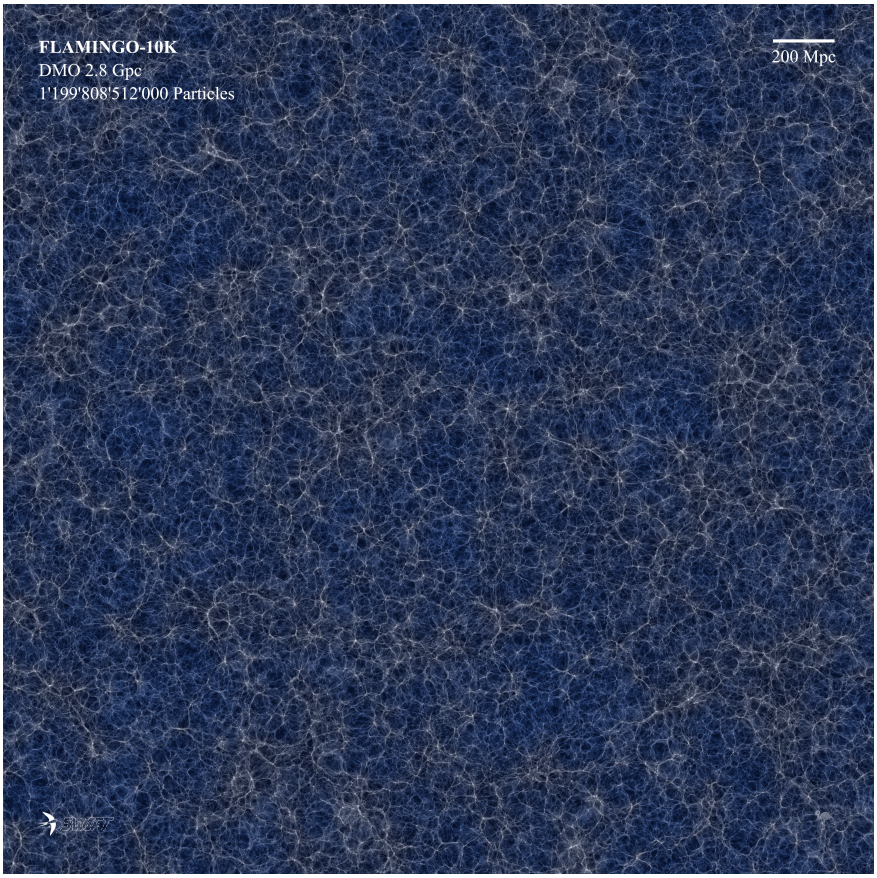

Figure 1.1: The large-scale structure of the Universe as predicted by the FLAMINGO-10k dark-matter-only (DMO) cosmological simulation (Schaller et al., in prep.; see also Chapter 3). This simulation was run by evolving over one trillion particles within a box measuring 2.8 cGpc per side, making it one of the largest simulations ever performed. A version of this image was turned into a puzzle – courtesy of Matthieu Schaller – and shared with the Leiden Observatory community. In assembling it, Ph.D. students at Leiden were reminded of Einstein's cosmological principle the hard way: the Universe gets surprisingly boring when you zoom out too far.

the Universe at the present epoch. The remaining components include dark energy (Λ, which can be associated with the cosmological constant in Einstein's field equations), cold dark matter (CDM), radiation, and neutrinos. While dark energy drives the accelerated expansion of the Universe at late times, cold dark matter – a non-luminous, collisionless form of matter – is essential for the formation and growth of cosmic structures. Although its precise nature remains unknown and direct detection has not yet been achieved, the gravitational influence of dark matter is indispensable for reconciling theoretical predictions with a wide range of astrophysical observations, including the dynamics of galaxies, gravitational lensing, and the large-scale clustering of matter.

Even though the Friedmann equations assume a perfectly smooth Universe, we know that in reality, it contains small Gaussian density perturbations. The origin of these fluctuations is still not fully understood – likely, they arise from quantum fluctuations in the very early Universe, which were stretched to macroscopic scales during a brief period of cosmic inflation. But we know for a fact that these fluctuations exist: we see them imprinted in the Cosmic Microwave Background (CMB), which offers a direct snapshot of the Universe at a redshift $z \approx 1100$. The exquisite measurements of the CMB – particularly by missions such as WMAP and Planck (Spergel et al. 2007; Planck Collaboration et al. 2014) – provide strong evidence for the statistical properties of these primordial fluctuations.

These small overdensities in the primordial density field act as the seeds from which all cosmic structures emerge. In the early Universe, these perturbations evolve linearly: fluctuations at different scales grow independently and proportionally to a common, time-dependent growth factor. Within this regime, linear perturbation theory provides an accurate analytic description of the evolution of the matter density field (e.g., Peebles 1980). As cosmic time progresses, however, overdensities grow under the influence of gravity and eventually reach the threshold at which linear theory ceases to be valid. This transition marks the onset of the non-linear regime of structure formation. Gravitational collapse proceeds anisotropically – typically beginning along the shortest axis of a perturbation – giving rise to the complex filamentary pattern known as the cosmic web (see Fig. 1.1; Bond et al. 1996). When matter collapses along all three spatial dimensions, it forms bound, virialized structures known as *halos*. These halos are made of dark matter, which collapses earlier than their baryonic counterparts due to its collisionless nature. Once halos form, they act as gravitational wells that attract baryonic gas, allowing it to cool, condense, and eventually form stars and galaxies (Barkana & Loeb 2001; Dayal & Ferrara 2018).

To study the non-linear regime of structure formation, cosmologists employ N-body simulations, which numerically evolve a system of particles under their mutual gravitational interactions. Since dark matter dominates the mass budget of the Universe and drives the formation of structures, these

simulations typically include only dark matter (and, in some cases, massive neutrinos). They are therefore commonly referred to as dark-matter-only simulations. In contrast, baryonic processes – such as gas dynamics, radiative cooling, star formation, and feedback from supernovae and AGN – introduce considerable physical complexity and are associated with significant modeling uncertainties (Vogelsberger et al. 2020). These effects become prominent mainly at the scale of dark matter halos, where non-gravitational forces play a critical role. On larger scales, however, the influence of baryons is subdominant, allowing the large-scale structure of the Universe to be accurately described using gravity alone.

Since the pioneering efforts in the early 1980s (e.g., Efstathiou et al. 1985; Davis et al. 1985), the field of N-body simulations has evolved significantly, driven by advances in algorithms and computational capabilities (Angulo & Hahn 2022). Modern simulations are able to capture the formation and evolution of structures with remarkable accuracy, extending from ∼Gpc scales down to the ∼kpc scale of subhalos. Figure 1.1 presents an example of the projected matter density field from the FLAMINGO-10k cosmological simulation (Schaller et al., in prep.). With more than 10^{12} dark matter (CDM) particles evolved in a 2.8 cGpc box, it represents one of the largest simulations ever run.

1.1.1 Dark matter halos as the building blocks of cosmic structure formation

By acting as gravitational wells that attract baryons, dark matter halos are the fundamental environments within which visible structures in the Universe originate. Infalling gas cools radiatively and condenses at the centre of halos, eventually giving rise to stars, galaxies, and supermassive black holes. Consequently, there exists a close connection between the hierarchical assembly of dark matter halos and the formation and evolution of galaxies. This correspondence forms the basis of theoretical frameworks such as semi-analytic models (SAMs) and semi-empirical approaches, which model galaxy formation and evolution by tracking the distribution and merging histories of halos and subhalos (i.e., satellite halos contained within a larger halo) across cosmic time (Somerville & Davé 2015; Lapi et al. 2025).

The distribution and evolution of (sub)halos can be extracted from N-body cosmological simulations using (sub)halo finder algorithms. These algorithms analyze the particle data output from simulations to identify gravitationally bound structures. Typically, halo finders first locate candidate halos based on density peaks or groups of particles connected in configuration, phase, or history space, and then apply an unbinding procedure to remove particles that are not gravitationally bound (Onions et al. 2012; Forouhar Moreno et al. 2025).

An alternative to explicitly identifying halos in simulations is provided by the halo model (e.g., Cooray & Sheth 2002). This empirical framework assumes that all matter resides in dark matter halos and uses analytic prescriptions for halo properties, abundances, and spatial distributions to statistically describe the large-scale matter field. Rather than tracking individual halos, the halo model predicts ensemble-averaged quantities – such as correlation functions or power spectra – by extending linear theory using analytic prescriptions (Asgari et al. 2023). While effective at quasi-linear scales ($r \gtrsim 10\,\mathrm{cMpc}$), the halo model becomes increasingly inaccurate at small scales, high redshifts, and large halo masses, due to its simplified assumptions about halo profiles, substructure, and non-linear effects (e.g., Mead & Verde 2021). These limitations make it unsuitable for the regimes explored in this thesis. For this reason, we rely on large-volume N-body simulations to extract accurate halo statistics in Chapters 2–5.

The most fundamental statistic describing the halo population is the halo mass function (HMF), which quantifies the comoving number density of halos as a function of mass. In its simplest analytical form, the HMF can be derived using the Press–Schechter formalism (Press & Schechter 1974). This approach assumes that halos form from regions in the initial density field where the linearly extrapolated density contrast, smoothed on some scale, exceeds a critical threshold for collapse. This allows one to relate the abundance of halos to the statistical properties of the initial Gaussian density field. While the Press–Schechter model captures the essential physics of hierarchical collapse, it relies on simplifying assumptions and underestimates halo abundances at both the low- and high-mass ends. Modern N-body simulations offer precise empirical descriptions of the HMF over a wide range of halo masses and redshifts, accounting for the full non-linear dynamics of structure formation (e.g., Tinker et al. 2008; Bocquet et al. 2016).

Another key property of halos is their spatial clustering. Because halos form from peaks in the initial density field, their distribution is biased relative to the underlying matter distribution. This phenomenon, known as cosmological halo bias, is scale-dependent in general, but on large (linear) scales, it is well described by a mass- and redshift-dependent bias factor.

The origin of halo bias can be understood through the statistics of Gaussian random fields. Rarer peaks – associated with more massive halos – require the constructive interference of more Fourier modes and are thus more clustered than typical regions. More quantitatively, a halo of mass M at redshift z corresponds to a peak in the smoothed linear density field whose height is given by $\nu(M, z) = \delta_c(z)/\sigma(M)$, where $\delta_c(z)$ is the critical linear overdensity for collapse, and $\sigma(M)$ is the standard deviation of the density field smoothed on the scale corresponding to mass M. Higher peak heights ($\nu \gg 1$) correspond to rarer, more strongly clustered halos. This implies that halo clustering strength increases with both halo mass and redshift. For instance, at fixed mass, halos forming at earlier times must come from

higher peaks, since the growth factor is smaller and fluctuations must be intrinsically larger to collapse by that time. Similarly, at fixed redshift, more massive halos form from rarer, higher peaks, and are therefore more strongly biased.

This connection between halo clustering and mass enables a powerful technique in galaxy formation studies: by comparing the observed clustering of a galaxy population to theoretical predictions for the clustering of halos, one can infer the typical mass of the halos that host those galaxies (e.g., Mo & White 1996). This provides crucial insight into the connection between galaxies and their large-scale environments. In Chapters 2-5, we will apply the same idea to connect quasars to halos and galaxies by using their measured clustering properties (see Sec. 1.3.2).

1.2 Galaxies and their central black holes

In 1925, Edwin Hubble used the period-luminosity relation of Cepheid variables – originally discovered by Henrietta Leavitt – to demonstrate that the Andromeda Nebula lies well beyond the boundaries of the Milky Way (Hubble 1925). This discovery resolved the "Great Debate" and marked the beginning of extragalactic astronomy: the Universe consists not just of stars within our own galaxy, but of countless other galaxies scattered across cosmic space (Trimble 1995).

One century later, our view of the cosmos has dramatically expanded. We now routinely observe hundreds of billions of galaxies, tracking their formation and evolution from the earliest epochs (up to $z \approx 14$, Carniani et al. 2024) to the present day. The classical picture of galaxies as isolated "island universes", a concept popularized by Immanuel Kant, has been replaced by a far more dynamic one. Galaxies are not self-contained or static – they are complex, interconnected ecosystems, shaped by both their internal processes and their interactions with the surrounding cosmic environment.

In recent years, theoretical models of galaxy formation have been complemented by the development of large-scale hydrodynamical simulations, which now serve as key tools for studying galaxy evolution in a cosmological setting. Landmark projects such as Illustris (Vogelsberger et al. 2014), EAGLE (Schaye et al. 2015), and IllustrisTNG (Nelson et al. 2019) have demonstrated that it is possible to reproduce a broad range of observed galaxy properties across cosmic time within large cosmological volumes ($100 - 300\,\mathrm{cMpc}$). These simulations go beyond N-body models by solving the coupled equations of gravity and hydrodynamics for baryonic matter, while also incorporating subgrid models for key processes such as star formation and feedback from supernovae and AGN. With the progressive refinement of such models, simulations have reached a stage where they can successfully reproduce numerous observables, including the stellar mass

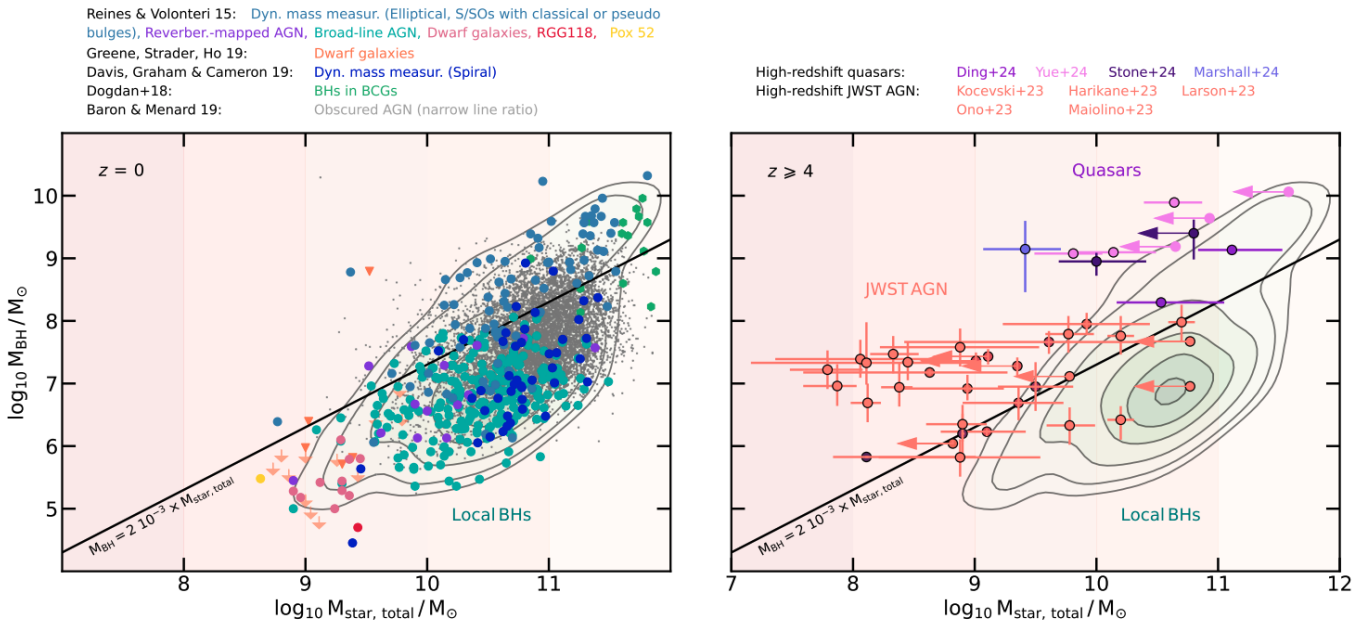

Figure 1.2: *Left:* Black hole mass–stellar mass relation in the local Universe, illustrating the overall connection between galaxy growth and the assembly of their central supermassive black holes (SMBHs). SMBH masses are derived using a range of observational techniques, including dynamical modeling, reverberation mapping, and virial estimates from broad emission lines. Different galaxy types and measurement methods are indicated with distinct colors and markers (measurements are taken from Reines & Volonteri 2015; Greene et al. 2020; Davis et al. 2019; Bogdán et al. 2018; Baron & Ménard 2019). *Right:* Same as the left panel, but for the high-redshift Universe ($z > 4$). Sources are divided between quasars (measurements from Ding et al. 2023; Stone et al. 2023; Yue et al. 2024a; Marshall et al. 2023) and JWST-discovered AGN candidates (see Sec. 1.3.4; Kocevski et al. 2024; Maiolino et al. 2024; Harikane et al. 2023; Ono et al. 2023; Larson et al. 2023). The contours represent the distribution of systems in the local Universe and are shown as a reference. Figure taken from Alexander et al. (2025).

function, star formation rates, morphologies, sizes, colors, and the spatial clustering of galaxies (Vogelsberger et al. 2020; Crain & van de Voort 2023).

One of the most significant insights to emerge from both theoretical models and cosmological hydrodynamical simulations is the central role played by supermassive black holes (SMBHs) in shaping the evolution of their host galaxies. Residing at galactic centers, SMBHs are far from being passive end-products of galaxy formation. Instead, they exert a profound influence on their large-scale environment through energetic feedback processes. In particular, AGN and quasar feedback – driven by gas accretion onto SMBHs – plays a pivotal role in regulating star formation, heating and ejecting gas, and ultimately quenching the growth of massive galaxies (Croton et al. 2006; Hopkins et al. 2006; Sijacki et al. 2007; Booth & Schaye 2009).

These feedback mechanisms are now recognized as essential components in explaining a wide range of observed galaxy properties. They help resolve long-standing discrepancies between theoretical predictions and observations, such as the cutoff in the high-mass end of the stellar mass function, the color bimodality of galaxies, and the existence of massive quiescent systems at relatively early cosmic epochs (Sazonov et al. 2005; Fabian 2012; Bower et al. 2006; Somerville & Davé 2015). By linking small-scale black hole accretion physics to large-scale galaxy evolution, AGN feedback has become a cornerstone of modern galaxy formation theory.

Perhaps the clearest observational evidence for the co-evolution of galaxies and their central black holes is the existence of empirical correlations between SMBH mass and several key galaxy properties – such as bulge mass, stellar mass, and circular velocity (Fig. 1.2, left panel). First identified about two decades ago (Magorrian et al. 1998; Gebhardt et al. 2000; Ferrarese & Merritt 2000), these relations imply that the assembly of SMBHs and galaxies is not independent, but regulated by coupled physical processes. As such, they provide key constraints for both semi-analytic models and cosmological simulations, informing prescriptions for black hole seeding, growth, and feedback (Sec. 1.2.2).

At the same time, the origin of these relations, particularly their emergence and evolution at high redshift, remains an open question and a key focus of ongoing research (Volonteri et al. 2021; Greene et al. 2020). Probing how these relations evolved across cosmic time can reveal when and how the coupling between SMBHs and their host galaxies was established, and what are the key drivers of this process. Recent high-redshift observations from JWST have opened a new observational window into this regime. Fig. 1.2 (right panel) presents a compilation of SMBH–host galaxy mass measurements from AGN and quasars at $z > 4$, offering early constraints on the redshift evolution of the scaling relation. Whether the normalization of this relation increases with redshift – suggesting that SMBHs outpace their hosts in early growth – or remains constant, is still a subject of considerable debate (Pacucci et al. 2023; Li et al. 2025).

In summary, the last few decades have marked a paradigm shift in our understanding of black holes: from abstract mathematical solutions of Einstein's equations to fundamental agents in shaping galaxies and the large-scale structure of the Universe.

1.2.1 Black holes: a journey through ten orders of magnitude in the mass spectrum

The history of black holes as astrophysical objects begins with one of the most remarkable discoveries in observational astronomy: quasars. In 1963, Maarten Schmidt investigated the radio source 3C 273 and realized that its optical spectrum contained redshifted hydrogen emission lines (Schmidt 1963). According to Hubble's law, this redshift implied a cosmological distance of several hundred cMpc, placing it far beyond the local Universe. Given this distance, its observed flux corresponded to a luminosity exceeding that of entire galaxies. Moreover, the rapid variability of its emission constrained the size of the emitting region to less than a parsec, implying an extraordinarily compact and dense energy source.

To account for such features, Edwin Salpeter and Yakov Zeldovich independently proposed in 1964 that the energy source powering quasars must be gravitational accretion of matter onto a massive, compact object – what we now call a supermassive black hole (Salpeter 1964; Zel'dovich & Novikov 1967). Donald Lynden-Bell further developed this idea in 1969, arguing that the infalling material would form a rotating disk, funnelling into what he described as a "Schwarzschild throat" (Lynden-Bell 1969). He went on to suggest that inactive galactic nuclei are simply the fossil remnants of once-luminous quasars, now harboring SMBHs at their cores.

Additional dynamical evidence began to support the existence of SMBHs. In 1970, Wolfe and Burbidge showed that the large stellar velocity dispersions observed in elliptical galaxy nuclei required a mass concentration far exceeding what could be attributed to normal stars (Wolfe & Burbidge 1970). They concluded that a central black hole as massive as $\sim 10^{10}\,\mathrm{M}_\odot$, or a swarm of smaller black holes, could account for the data. The first concrete dynamical detection of such a massive dark object came in 1978 in the galaxy M87, where the core was inferred to host a $\sim 5 \times 10^9\,\mathrm{M}_\odot$ black hole (Sargent et al. 1978). Similar measurements in other galaxies soon followed (e.g., Kormendy 1988).

Closer to home, Lynden-Bell and Rees hypothesized in 1971 that the Milky Way's center should host a massive black hole (Lynden-Bell & Rees 1971). This idea gained traction after the discovery of the compact, bright radio source Sagittarius A* (Sgr A*) in 1974 by Balick & Brown (1974). Follow-up infrared observations over the following decades measured the orbits of individual stars near the Galactic Center with exquisite precision (Eckart & Genzel 1996; Ghez et al. 2008). These showed that Sgr A* must

contain a mass of $\sim 4 \times 10^6\,M_\odot$ confined within a region smaller than the Solar System – evidence so compelling that it earned the 2020 Nobel Prize in Physics for Genzel, Ghez, and Penrose.

Today, it is well established that SMBHs are ubiquitous in the local Universe. Observational surveys show that essentially all galaxies with a bulge component host a central SMBH (Kormendy & Ho 2013). In recent years, the Event Horizon Telescope has provided even more direct evidence: the first resolved images of the event horizons of two SMBHs, in M87 (Event Horizon Telescope Collaboration et al. 2019) and our own Milky Way (Event Horizon Telescope Collaboration et al. 2022).

In parallel to the discovery of quasars and the growing realization that SMBHs reside in galactic nuclei, a different class of black holes was being uncovered with the rise of X-ray astronomy. In the early 1970s, observations with balloon-borne and satellite-based detectors revealed bright X-ray sources in the Milky Way. Among the most notable was Cygnus X-1, whose X-ray variability and association with a massive O-type star pointed to the presence of an unseen, compact companion. Detailed dynamical studies confirmed that the mass of this dark object exceeded the theoretical limit for a neutron star, providing the first compelling evidence for a stellar-mass black hole (Bolton 1972). These black holes are now understood to form as the end products of massive stellar evolution, when the core of a massive star collapses under its own gravity after exhausting its nuclear fuel.

While a handful of stellar-mass black holes were known from X-ray binaries in the late 20th century, the true diversity and abundance of this population remained elusive until the advent of gravitational wave astronomy. Beginning in 2015 with the landmark detection of GW150914, the LIGO and Virgo observatories have opened a new window onto the Universe, directly detecting the mergers of binary black hole systems through their gravitational wave emission (Abbott et al. 2016). These discoveries unveiled a surprising population of stellar-mass black holes, with masses ranging from a few to over 100 solar masses – challenging preexisting models of stellar evolution and compact object formation (Abbott et al. 2019). The growing catalog of gravitational wave events now offers an independent, dynamical probe of black hole demographics, complementing electromagnetic observations and revealing regions of parameter space previously inaccessible.

Taken together, black holes span over ten orders of magnitude in mass, from a few solar masses to tens of billions. While solid observational evidence remains limited to the regimes of stellar-mass ($\sim 1 - 100\,M_\odot$) and supermassive ($\sim 10^6 - 10^{10}\,M_\odot$) black holes, the mass distribution of these systems is thought to form a continuum, shaped by diverse evolutionary and growth pathways and possibly by multiple formation channels. The elusive population of intermediate-mass black holes (IMBHs; $\sim 10^2 - 10^5\,M_\odot$) remains poorly constrained observationally, but evidence for their existence is gradually accumulating. This includes the detection of very massive mergers

of stellar-mass black holes (The LIGO Scientific Collaboration et al. 2025), the identification of candidate low-luminosity AGN potentially powered by IMBHs (Greene et al. 2020), and alternative signatures such as tidal disruption events (Zhang et al. 2025) or dynamical studies of dense stellar systems, with recent claims involving systems like ω Centauri (Häberle et al. 2024).

1.2.2 Quasars as tracers of SMBH growth

The journey of black holes across the mass spectrum remains largely mysterious – particularly at the low-mass end, where formation pathways and early evolution are still poorly constrained by observations. At the opposite end of the spectrum, however, the formation and evolution of SMBHs is illuminated by a simple and elegant argument first articulated by Soltan (1982). The "Soltan argument" asserts that the same accretion processes powering luminous quasars naturally account for the buildup of SMBH mass over cosmic time.

The key idea is as follows: when gas is accreted onto a black hole at a rate $\dot{M}_{\rm acc}$, a fraction ϵ (known as *radiative efficiency*) of its rest-mass energy is converted into radiation. This results in a bolometric luminosity given by:

$$L_{\rm bol} = \epsilon \dot{M}_{\rm acc} c^2. \tag{1.1}$$

General relativity predicts values of $\epsilon \approx 0.05{-}0.3$, depending on the spin of the black hole. This efficiency far exceeds that of nuclear fusion and gives rise to the extreme luminosities of quasars, with $L_{\rm bol} \approx 10^{45}{-}10^{49}\,{\rm erg\,s^{-1}}$.

At the same time, the remainder of the accreted mass – i.e., the fraction not radiated away – contributes to the growth of the black hole itself:

$$\dot{M}_{\rm BH} = (1-\epsilon)\dot{M}_{\rm acc}. \tag{1.2}$$

By combining the two above equations, we can directly link the observed luminosity of quasars to the rate at which black holes grow during their active accretion phases, with the only conversion parameter being the radiative efficiency.

What Soltan (1982) recognized is that if one integrates the total light emitted by all quasars over cosmic time, and converts the resulting energy into an accreted mass using a plausible value of ϵ, the result should match the local SMBH mass density inferred from galaxy bulge–black hole scaling relations. For a typical efficiency of $\epsilon \approx 0.1$, the agreement is striking – providing strong evidence that most of the mass in today's SMBHs was assembled through luminous accretion.

This argument leads to a compelling picture in which quasars are direct signposts of black hole growth. The radiation we observe from distant quasars reflects the very process by which SMBHs gain mass. According to this view,

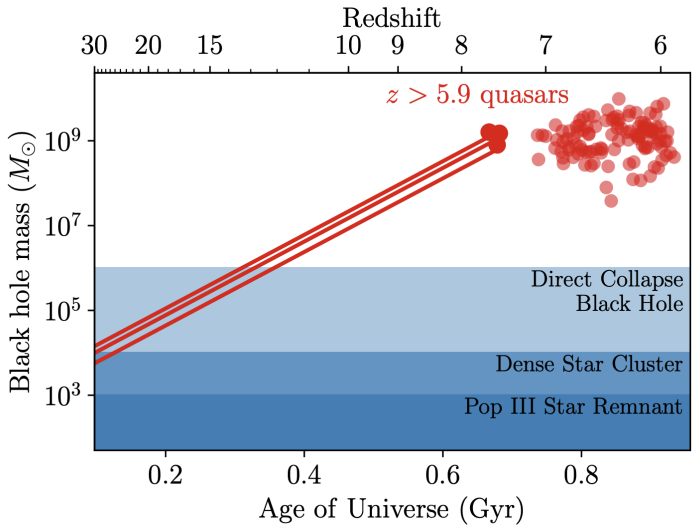

Figure 1.3: Growth histories of SMBHs in the early Universe. Data points indicate black hole masses inferred from observations of quasars at $z > 5.9$. Solid lines show the corresponding growth tracks for the three most distant quasars, assuming continuous, Eddington-limited accretion. Even under this idealized scenario, the observed SMBH masses can only be reached if the initial seed mass $M_{\rm seed}$ is at least $\sim 10^4\,{\rm M}_\odot$ by $z \approx 30$. The shaded blue regions illustrate the typical mass ranges associated with different SMBH seed formation channels. Figure adapted from Fan et al. (2023).

luminous quasars trace the peak phases of SMBH accretion, and their cosmic distribution encodes the history of black hole growth across the Universe. In this way, the Soltan argument establishes a direct connection between the quasar population observed at high redshift and the "relic" SMBHs we find in the centers of galaxies today – as first predicted by Lynden-Bell (1969).

An important consequence of accretion-powered growth is that the radiation emitted by infalling material exerts an outward force – radiation pressure – that counteracts gravity. This interplay naturally sets an upper bound on the accretion rate, beyond which radiation pressure would halt further inflow of gas. This theoretical limit is known as the Eddington limit, and it defines the maximum luminosity an accreting black hole can sustain under the assumption of spherical symmetry and steady inflow.

The Eddington luminosity is derived by equating the outward radiation force on electrons (via Thomson scattering) with the inward gravitational pull on protons:

$$L_{\rm Edd} = \frac{4\pi G M_{\rm BH} m_p c}{\sigma_T} \approx 1.3 \times 10^{38} \left(\frac{M_{\rm BH}}{{\rm M}_\odot}\right) {\rm erg\,s^{-1}}, \tag{1.3}$$

where G is the gravitational constant, m_p is the proton mass, σ_T is the Thomson cross-section, and $M_{\rm BH}$ is the black hole mass. Because $L_{\rm Edd} \propto M_{\rm BH}$, the maximum allowed accretion rate increases linearly with the black hole's mass.

Quasars are observed to radiate at a wide range of Eddington ratios, defined as the ratio of bolometric luminosity to the Eddington luminosity, $\eta = L_{\rm bol}/L_{\rm Edd}$, with the peak of the distribution ranging between $\eta \approx 0.1-1$ depending on the quasars' luminosity and redshift (Wu & Shen 2022). For theoretical modeling, it is common to assume that SMBHs grow at a constant Eddington ratio η, which allows one to derive a characteristic exponential growth law. If a black hole begins with a seed mass $M_{\rm seed}$ at time $t_{\rm seed}$ and accretes continuously at a fixed η, its mass at a later time t is given by:

$$M_{\rm BH}(t) = M_{\rm seed}\, e^{(t-t_{\rm seed})/\tau_{\rm Salp}}, \tag{1.4}$$

where $\tau_{\rm Salp}$ is the Salpeter time, the e-folding timescale for black hole growth under Eddington-limited accretion:

$$\tau_{\rm Salp} \approx 45\,{\rm Myr}\left(\frac{\epsilon}{0.1(1-\epsilon)}\right)\left(\frac{\eta}{1}\right)^{-1}. \tag{1.5}$$

This simple model offers valuable intuition: SMBHs can, in principle, grow from light seed BHs – e.g., $M_{\rm seed} \approx 10^2 - 10^3\,{\rm M}_\odot$, formed from the collapse of the first generation of stars (PopIII stars, Heger et al. 2003) – to billions of solar masses within less than a billion years if accretion proceeds continuously near the Eddington rate.

However, the model also rests on idealized assumptions that likely break down in realistic environments. The complex interplay between accretion and feedback processes makes it unlikely that SMBHs accrete continuously at the same rate. Instead, simulations and physical models show that SMBHs likely grow during discrete, episodic phases (e.g., Novak et al. 2011; Anglés-Alcázar et al. 2015; Trinca et al. 2024). This is often parametrized by introducing an effective duty cycle for quasar activity, which accounts for the fraction of time SMBHs spend in radiatively efficient accretion phases, as opposed to quiescent or inefficient states (Shankar et al. 2009; Pacucci & Loeb 2022). As discussed in Sec. 1.3.2, indirect probes of this intermittent behavior of quasar activity are recently becoming available in the early Universe, opening up the possibility of testing more realistic growth histories against observations (see also Chapter 5).

Additionally, purely accretion-driven models neglect the contribution of black hole mergers. When two SMBHs merge, the resulting remnant has a mass that is approximately equal to the sum of the progenitor masses – reduced by the small fraction of energy radiated away as gravitational waves during the coalescence. While mergers do not alter the integrated black hole mass density that enters the Soltan argument, they can significantly

affect the individual growth histories of SMBHs. This contribution may be particularly important at high redshift and low masses – where merger rates are high – and at low redshift for the most massive black holes whose accretion has been quenched (Volonteri et al. 2003; Pacucci & Loeb 2020; Zou et al. 2024).

1.2.3 The high-redshift frontier

As observational capabilities have pushed the detection of quasars to increasingly earlier cosmic times, a striking realization has emerged: although the number density of quasars declines steeply with redshift (Figure 1.4), some SMBHs with masses $M_{\rm BH} \gtrsim 10^9\,{\rm M}_\odot$ are already in place within the first few hundred million years after the Big Bang. These objects, observed at redshifts $z \gtrsim 6$, rival the most massive black holes found in the centers of present-day galaxies (Fan et al. 2023).

The discovery of ever earlier quasars powered by billion-solar-mass black holes – the current record-holder is at $z \approx 7.64$ (Wang et al. 2021) – has significantly increased the tension with standard models of SMBH formation and growth. The core challenge is straightforward: there appears to be insufficient cosmic time for these black holes to grow from the $\sim 100\,{\rm M}_\odot$ seeds expected from PopIII stellar remnants (Heger et al. 2003) – even under the most optimistic scenario of continuous, Eddington-limited accretion (Haiman & Loeb 2001). This issue is illustrated in Figure 1.3, which compares the expected growth tracks for Eddington-limited accretion to the observed SMBH masses at high redshift.

To resolve this challenge, several massive seed formation scenarios have been proposed (Inayoshi et al. 2020). One leading pathway is the direct collapse of pristine gas clouds into black holes with masses in the range 10^4–10^6 ${\rm M}_\odot$, under specific conditions that suppress fragmentation and prevent star formation (Bromm & Loeb 2003; Volonteri et al. 2008; Latif & Ferrara 2016; Lupi et al. 2021). Another possibility is the runaway collapse of dense stellar clusters, particularly those composed of PopIII stars, where repeated stellar collisions and mergers can lead to the formation of IMBHs (Omukai et al. 2008; Devecchi & Volonteri 2009). These scenarios ease the growth timescale constraints by starting with more massive seeds, but they rely on specific environmental conditions and remain difficult to test observationally.

An alternative route to alleviating the timing problem is to relax the assumption of Eddington-limited accretion. If black holes can grow through super-critical accretion – i.e., with accretion rates higher than the Eddington rate, $\dot{M}_{\rm Edd} = L_{\rm Edd}/\epsilon c^2$ – the stringent time constraints for SMBH growth are considerably relaxed (Volonteri & Rees 2006). Numerical simulations suggest that in dense, gas-rich environments, black holes can exceed the classical Eddington rate under specific physical conditions. Mechanisms

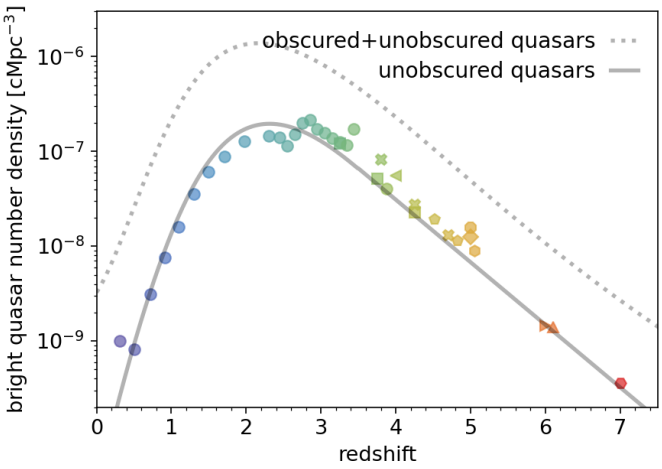

Figure 1.4: Evolution of the number density of bright quasars as a function of redshift. The solid line represents the number density of UV-luminous quasars that are brighter than $M_{1450} < -25.7$, adapted from the global QLF evolution model of Kulkarni et al. (2019) as described in Pizzati et al. (2025). Data points are obtained by integrating UV-optical QLF models at different redshifts. The dotted line shows the number density of bright quasars as estimated from the bolometric QLF model of Shen et al. (2020), by assuming a $L_{\rm bol}$ threshold consistent with the UV magnitude limit mentioned above. The gap between the solid and dotted lines arises from the UV-obscured quasar population. Figure adapted from Schindler et al. (2023) and Pizzati et al. (2025, Chapter 4).

such as photon trapping, slim accretion disks, and anisotropic radiation fields allow accretion to proceed at super-Eddington rates without unbinding the inflowing material (Sądowski et al. 2014; Volonteri et al. 2015; Inayoshi et al. 2020). However, because such accretion is expected to be radiatively inefficient, direct observational confirmation remains challenging. So far, empirical evidence is limited to a few high-redshift quasars with Eddington ratios modestly above unity (Wu et al. 2022). Nonetheless, a growing body of work is investigating indirect signatures of super-critical accretion, either through spectral diagnostics of AGN (Pacucci & Narayan 2024; Lambrides et al. 2024; Liu et al. 2025; Quadri et al. 2025) or through empirical arguments based on quasar growth timescales and duty cycles (Davies et al. 2019; Eilers et al. 2021, 2024).

Despite substantial theoretical efforts to uncover the growth history of SMBHs, progress remains limited by two persistent challenges: the difficulty of constructing predictive, first-principles models (see Sec. 1.4) and the lack of direct observational constraints beyond the (relatively uncertain) black hole mass estimates. At present, the problem remains highly degenerate – vastly different combinations of seed mass, accretion rate, duty cycle, and

merger history can be fine-tuned to match the observed SMBH masses at a given redshift. As a result, the mere existence of billion-solar-mass black holes in the early Universe is a necessary, but insufficient, condition to distinguish between competing formation and growth scenarios.

Encouragingly, recent and upcoming observations promise to break this impasse and shed new light on SMBH evolution across cosmic time. New AGN candidates uncovered at even higher redshifts by JWST are already putting pressure on existing evolutionary models. Although the nature of these candidates remains uncertain (see Sec. 1.3.4), the advent of wide-field missions such as Euclid and the Roman Space Telescope will soon provide statistically robust samples of luminous quasars at the highest redshifts. At the same time, quasar observables – including luminosity functions, clustering measurements, and proximity zone sizes – are being extended to earlier epochs, offering complementary constraints on black hole accretion physics and environments. Looking further ahead, gravitational wave detections from merging SMBHs will open a fundamentally new observational window into the merger-driven component of black hole growth.

In the following section, I review these recent advancements and highlight the key observational tools – particularly those most relevant to the focus of this thesis – that are currently shaping our understanding of SMBH formation and growth across cosmic time.

1.3 Observations: the evolution of quasars and SMBHs across cosmic times

A major leap forward in quasar studies came with the advent of optical wide-field spectroscopic surveys, which transformed quasars from rare, exotic sources into a population with robust statistical power. Landmark efforts such as the Sloan Digital Sky Survey (SDSS; York et al. 2000), the 2dF QSO Redshift Survey (2QZ; Croom et al. 2004), the Baryon Oscillation Spectroscopic Survey (BOSS; Dawson et al. 2013), and its successor, the extended BOSS (eBOSS; Dawson et al. 2016), have collectively catalogued hundreds of thousands of UV-bright quasars across a wide redshift range. These surveys have provided an unprecedented view of the statistical properties and cosmic evolution of quasars and their central SMBHs.

In parallel, multi-wavelength observations have significantly expanded the AGN census beyond optically selected quasars. Owing to their broadband emission, AGN can be detected across the entire electromagnetic spectrum, and surveys at other wavelengths – X-ray missions (e.g., Chandra, XMM-Newton), radio surveys (e.g., FIRST, NVSS, LOFAR), and mid-infrared campaigns (e.g., Spitzer, WISE) – have uncovered substantial populations of AGN that are obscured in the UV-optical. These datasets have been

instrumental in tracing black hole accretion across a wide range of host galaxy environments and evolutionary stages. Together, they provide a critical foundation for building a more complete and less biased picture of SMBH growth across cosmic history (Padovani et al. 2017).

1.3.1 The quasar luminosity function

The most basic metric for characterizing the demographic properties of the quasar population is the quasar luminosity function (QLF). The QLF describes the comoving number density of quasars as a function of luminosity and has been extensively measured across multiple wavelengths and over a wide range of redshifts (e.g., Boyle et al. 2000; Richards et al. 2006; Ross et al. 2013; Akiyama et al. 2018).

Empirically, the QLF is typically modeled as a broken power law, with the normalization, faint-end slope, and characteristic break luminosity evolving strongly with redshift. This evolution reflects the cosmic history of black hole accretion, with a pronounced peak at $z \sim 2-3$ – the so-called "cosmic noon" – when both quasar activity and global star formation reach their maximum (Shen et al. 2020). The striking similarity between the redshift evolution of the QLF and that of the cosmic star formation rate density (Ciotti et al. 2003) supports the widely discussed scenario of co-evolution between SMBHs and their host galaxies (Merloni & Heinz 2008; Heckman & Best 2014). Figure 1.4 illustrates the evolution of the bright quasar population across cosmic time, highlighting its rise from the epoch of reionization, peak activity around cosmic noon, and subsequent decline.

The most robust constraints on the QLF come from optical and UV-selected quasar samples, where the luminosity function is often expressed in terms of absolute UV magnitude (e.g., M_{1450}; Kulkarni et al. 2019). However, these measurements are inherently biased toward unobscured quasars, as obscuration from dust and gas can significantly attenuate emission in the UV and optical bands. This bias complicates the interpretation of QLF measurements, particularly because the fraction of obscured AGN is observed to vary with both luminosity and redshift (Aird et al. 2015; Buchner et al. 2015). These effects introduce systematic uncertainties when comparing observations with theoretical models, which typically predict intrinsic, bolometric luminosities.

To overcome these limitations, recent efforts have focused on constructing multi-wavelength AGN samples that combine X-ray, mid-infrared, UV-optical, and radio observations. These datasets are essential for recovering obscured quasars that are systematically missed in UV-only surveys. In particular, X-ray data allow for population-level obscuration corrections through measurements of hydrogen column densities (Ueda et al. 2014), enabling estimates of intrinsic AGN luminosities even for heavily absorbed systems. By applying these corrections and synthesizing observations across

multiple bands, several studies have reconstructed the bolometric QLF, providing a more comprehensive benchmark for models of black hole growth (Hopkins et al. 2007; Shen et al. 2020). In Figure 1.4, we compare a UV-selected QLF model (solid line) with a bolometric QLF derived from multi-wavelength data (dashed line). While these bolometric reconstructions offer a substantially improved census of AGN activity, significant uncertainties persist – especially at high redshift, where obscuration properties remain poorly constrained and the number of detected sources is still limited.

1.3.2 Quasar clustering and the duty cycle of quasars

In addition to the QLF, another key statistical observable for characterizing quasars in a cosmological context is their large-scale clustering. As discussed in Section 1.1.1, the ΛCDM paradigm predicts a strong dependence of halo clustering on mass. This implies that measuring the clustering strength of a population provides a powerful way to infer the characteristic mass of its host dark matter halos. By comparing the clustering amplitude of quasars to that of halos across a range of masses, one can constrain the typical environments in which quasars reside. In Chapters 2 and 3, we will build on this approach by jointly modeling the QLF and quasar clustering to infer the full mass distribution of quasar host halos – a quantity we refer to as the quasar–host mass function (QHMF).

The advent of large spectroscopic quasar surveys has enabled precise measurements of the quasar two-point auto-correlation function, the most direct probe of quasar clustering on cosmological scales. Numerous studies have characterized this clustering across a wide range of redshifts (e.g., Porciani et al. 2004; Croom et al. 2005; Porciani & Norberg 2006; Shen et al. 2007; da Ângela et al. 2008; Ross et al. 2009; White et al. 2012; Eftekharzadeh et al. 2015), consistently finding that quasars typically inhabit dark matter halos with masses around 10^{12}–$10^{13}\,\mathrm{M}_{\odot}$. This characteristic halo mass appears to be largely independent of quasar luminosity and evolves only mildly with redshift (see Figure 1.5). A possible exception to this is the large host halo mass inferred by Shen et al. (2007) at $z \approx 4$, which suggests a rapid evolution of the quasar properties at high redshift and provides very tight constraints on the inferred host mass distribution (Pizzati et al. 2024). Chapters 2 and 3 discuss in detail the implications of this measurement, building up on previous work from White et al. (2008); Wyithe & Loeb (2009); Shankar et al. (2010).

Interestingly, quasar clustering measurements not only constrain the typical mass of quasar host halos but also offer insights into the integrated timescale of quasar activity by estimating the quasar *duty cycle* (Martini & Weinberg 2001; Haiman & Hui 2001). The concept is illustrated in Figure 1.6: if SMBH accretion proceeds as a stochastic process, then the observed quasar population at any given epoch represents a random, luminous subset of the

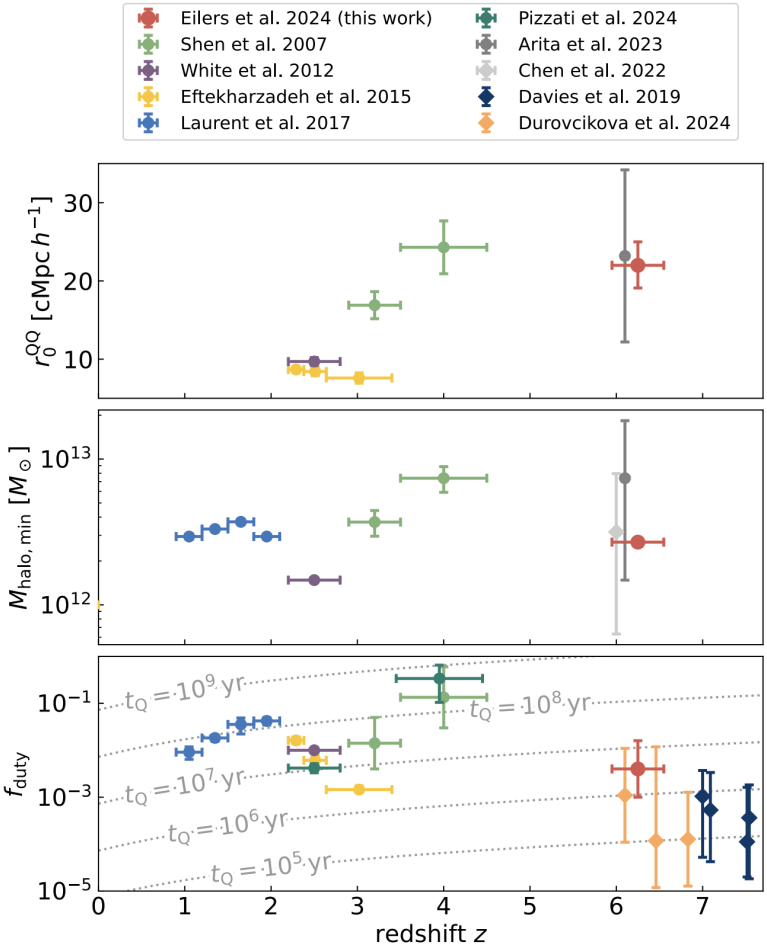

Figure 1.5: Redshift evolution of three key quasar properties: the autocorrelation length (top), host dark matter halo mass (middle), and duty cycle (bottom), as a function of redshift. Measurements at $z \approx 6$ are all based on recent work and obtained using different methods. The halo mass estimate from Chen et al. (2022) is based on transmitted flux measurements along quasar sightlines, and the duty cycle measurements from Davies et al. (2019); Ďurovčíková et al. (2024) are obtained from Lyα damping wing analyses. The remaining data are based on clustering measurements: Arita et al. (2023) measured the auto-correlation function of faint $z \approx 6$ quasars, while Eilers et al. (2024) used JWST WFSS observations to estimate the quasar-galaxy cross-correlation function at the same redshift. Gray dotted lines in the bottom panel correspond to constant quasar lifetimes. The results show that the characteristic host halo mass of quasars sits between $\sim 10^{12}\,\mathrm{M}_\odot$ and $\sim 10^{13}\,\mathrm{M}_\odot$ at all redshifts. The corresponding duty cycle, however, shows a significant redshift evolution. At $z \gtrsim 6$, f_{duty} is found to be $\lesssim 1\%$ using independent methods. Figure taken from Eilers et al. (2024).

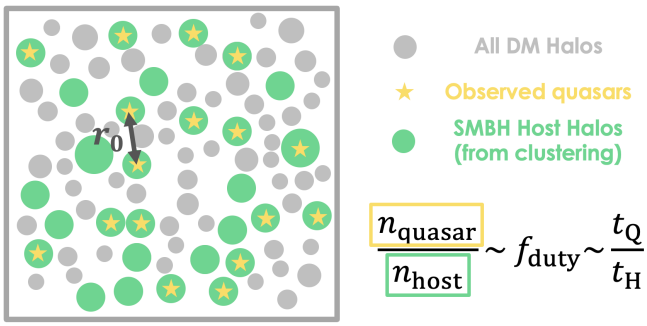

Figure 1.6: Schematic illustration of how quasar clustering measurements can be used to infer the quasar duty cycle. The full population of dark matter halos is shown as gray circles. Quasars (yellow stars) occupy only a subset of these halos, representing a stochastic sampling of the underlying SMBH population. By measuring the clustering of quasars, one can infer the typical mass – and hence number density – of their host halos (highlighted in green). Comparing the observed number density of quasars ($n_{\rm quasar}$) to the number density of similarly clustered halos ($n_{\rm hosts}$) yields an estimate of the quasar duty cycle: the average fraction of time a SMBH is observed as an active quasar. This duty cycle is commonly expressed as the ratio between the integrated quasar lifetime, $t_{\rm Q}$, and the cosmic timescale over which halos exist, approximated by the Hubble time, $t_{\rm H}$.

full SMBH population. Subsampling a population does not change its clustering: hence, by measuring the clustering of quasars we can infer the clustering of the dark matter halos hosting SMBHs. Using the connection between clustering and halo mass, we can then infer the characteristic mass and number density of these SMBH-host halos. We are implicitly assuming here that all massive halos host a SMBH (which can be either active or dormant) at their center, as it is the case in the local Universe. Comparing the number density of SMBH hosts ($n_{\rm host}$) to the observed number density of quasars ($n_{\rm quasar}$) yields the fraction of SMBHs that are active (i.e., visible as quasars) at a given time. This fraction corresponds to the average time a black hole spends in an active, luminous quasar phase over cosmic time: the so-called quasar duty cycle ($f_{\rm duty}$).

Recent efforts have extended clustering and duty cycle measurements into the epoch of reionization, a long-sought goal given the importance of understanding the environments of early quasars. While many studies have attempted to assess whether high-redshift quasars reside in overdense regions (e.g., Kim et al. 2009; Simpson et al. 2014), the first robust measurements of quasar clustering at $z \gtrsim 6$ have only recently emerged. These include the quasar auto-correlation analysis by Arita et al. (2023), based on faint quasars from the SHELLQs survey, and the quasar–galaxy cross-correlation study by Eilers et al. (2024), enabled by JWST's Wide Field Slitless Spectroscopy (WFSS) mode. The primary focus of Chapter 3 is to model these

measurements[2] and study their implications for quasar activity and SMBH growth in the early Universe. Intriguingly, the inferred duty cycle at $z \sim 6$ is $f_{\rm duty} \lesssim 1\%$, in agreement with independent estimates of quasar activity timescales from Lyα damping wing and proximity zone analyses (Davies et al. 2019; Ďurovčíková et al. 2024). This poses a challenge to standard scenarios of continuous, Eddington-limited black hole growth that are often invoked to explain the rapid emergence of $\gtrsim 10^9\,{\rm M}_\odot$ SMBHs in the early Universe.

1.3.3 SMBH mergers and gravitational waves

While electromagnetic observations of quasars trace the accretion-driven growth of SMBHs, gravitational wave (GW) observatories offer a complementary probe by directly accessing the merger-driven channel of black hole growth. As discussed in Sec. 1.2.1, ground-based GW detectors such as LIGO and Virgo have already provided a wealth of information about the stellar-mass black hole population through detections of compact binary coalescences (Abbott et al. 2023). In contrast, progress in the regime of SMBHs is more recent, but has accelerated markedly with the advent of pulsar timing array (PTA) experiments and will mature substantially in the next decade.

A landmark step forward has been the recent detection of a stochastic gravitational wave background (GWB) by multiple PTA collaborations, including NANOGrav (Agazie et al. 2023), the European PTA (EPTA Collaboration et al. 2023), the Parkes PTA (Reardon et al. 2023), and the Chinese PTA (Xu et al. 2023). These detections reveal a common-spectrum red noise process in pulsar timing residuals with evidence for spatial correlations consistent with the Hellings & Downs (1983) signature expected from gravitational waves in general relativity (Burke-Spolaor et al. 2019). The detected GWB is broadly consistent with the combined emission from inspiraling supermassive black hole binaries, typically with masses of order $\sim 10^8$–$10^{10}\,{\rm M}_\odot$ at redshifts $z \lesssim 2$. This detection provides the first direct GW evidence for the prevalence of SMBH mergers in the nanohertz frequency regime, marking a pivotal step for the field of SMBH evolution.

Looking ahead, PTAs are expected to move beyond statistical detections of a stochastic background to the resolution of individual SMBH binary systems. These future detections will be most sensitive to the most massive binaries ($M_{\rm tot} \gtrsim 10^9\,{\rm M}_\odot$) at relatively low redshifts ($z \lesssim 1$), and could enable the measurement of dynamical properties such as orbital eccentricity, mass ratios, and the nature of the merger environment. Concurrently, improvements in PTA sensitivity will enhance constraints on the unresolved

[2] In Appendix D of Chapter 3, I demonstrate that the halo mass and duty cycle estimates reported by Arita et al. (2023) are subject to methodological issues and are therefore unreliable.

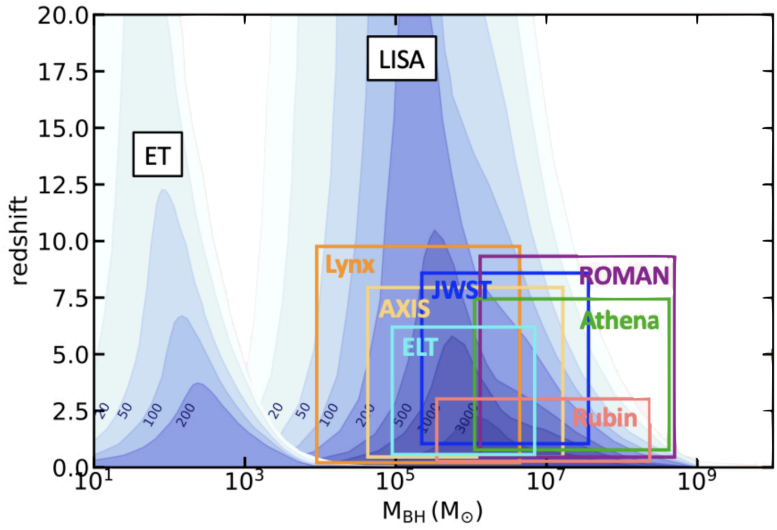

Figure 1.7: A broad overview of the black hole mass–redshift landscape and the observational capabilities expected to probe it. The figure shows the sensitivity ranges (i.e., the expected signal-to-noise curves for non-spinning binaries with mass ratio 0.5) of various gravitational wave (GW) observatories, such as LISA and future third-generation ground-based interferometers like the Einstein Telescope (ET), for detecting black hole mergers across a wide range of masses ($\sim 10^1$–$10^7\,M_\odot$) and cosmic epochs. These GW detectors will enable full-sky surveys, reaching from the local Universe to the era of the first black holes. Overlaid are the approximate reach of current and planned electromagnetic (EM) facilities – such as JWST, Roman, Rubin, the ELT, and next-generation X-ray observatories like Athena, LynX, and AXIS – highlighting the synergy between EM and GW observations. Taken from Volonteri et al. (2021).

gravitational wave background, offering a critical test of theoretical models of SMBH evolution. Intriguingly, several recent studies have reported emerging discrepancies between the amplitude of the detected background and predictions from leading semi-analytic and hydrodynamic models of SMBH assembly (e.g., Lapi et al. 2025). These tensions may reflect previously unmodeled physical processes, such as stalling of SMBH binaries due to inefficient hardening, coupling with circumbinary gas disks, or inaccuracies in merger rate prescriptions. As PTA datasets continue to grow in precision and temporal coverage, they will provide an increasingly powerful probe of the physics driving SMBH mergers and their role in cosmic structure formation.

At the opposite end of the SMBH mass spectrum lies the future space-based mission LISA (Laser Interferometer Space Antenna). Unlike PTAs, which are sensitive to the mergers of the most massive SMBHs at low redshift, LISA will probe the coalescence of lower-mass SMBHs and IMBHs

in the range 10^4–$10^7\,M_\odot$, reaching out to redshifts as high as $z \gtrsim 10$ with exceptional signal-to-noise. This makes LISA uniquely suited to explore the early formation and assembly of SMBHs, as well as the long-sought IMBH population. In particular, LISA will offer key insights into seed formation channels, early merger rates, and black hole occupation fractions in low-mass galaxies – regimes currently inaccessible to electromagnetic or PTA observations. Numerous studies have forecasted LISA's potential to constrain black hole demographics and binary environments (e.g., Sesana et al. 2007; Tanaka & Haiman 2009; Amaro-Seoane et al. 2023; Wang et al. 2025), but the field remains highly uncertain, with predicted detection rates spanning several orders of magnitude.

Figure 1.7 offers a schematic view of the observational landscape, mapping the redshift and black hole mass ranges accessible to current and upcoming gravitational wave and electromagnetic observatories. Alongside LISA, it includes the Einstein Telescope (ET) as a representative of the planned third generation (3G) of ground-based GW interferometers. These instruments will extend sensitivity to stellar-mass/IMBH mergers at high redshift, complementing LISA's reach and contributing to a unified picture of black hole growth across cosmic history. The design and associated challenges of 3G detectors are discussed in more detail in Chapter 6.

1.3.4 New challenges in the JWST era: the nature of "little red dots" and other broad-line AGN

The launch of the James Webb Space Telescope (JWST) has ushered in a transformative era for the study of AGN and quasars at high redshift. Thanks to its unprecedented sensitivity in the infrared, JWST can detect AGN that were previously invisible to traditional rest-frame UV and optical surveys, which until now have dominated our view of the AGN population during the epoch of reionization (Fan et al. 2023).

The first few years of observations with JWST have indeed uncovered a surprisingly rich population of faint AGN candidates at $z \approx 4$–10 (e.g., Harikane et al. 2023; Maiolino et al. 2024; Übler et al. 2023; Kocevski et al. 2023; Matthee et al. 2024b; Greene et al. 2024; Bogdán et al. 2024). Many of these sources are identified via the presence of broad rest-frame optical emission lines such as Hα or Hβ, accessible for the first time at high redshift thanks to JWST's NIRSpec and NIRCam instruments. These features enable black hole mass estimates of $M_{\rm BH} \gtrsim 10^{6-8}\,M_\odot$ and bolometric luminosities of $L_{\rm bol} \gtrsim 10^{43-46}\,{\rm erg\,s^{-1}}$, extending the census of actively accreting SMBHs well below the luminosities of previously known quasars at comparable redshifts. The emergence of this population opens new avenues to address key questions in early black hole and galaxy evolution, including the co-evolution of SMBHs and their hosts (e.g., Pacucci et al. 2023), the contribution of faint AGN to hydrogen reionization (e.g., Dayal et al. 2024; Madau et al.

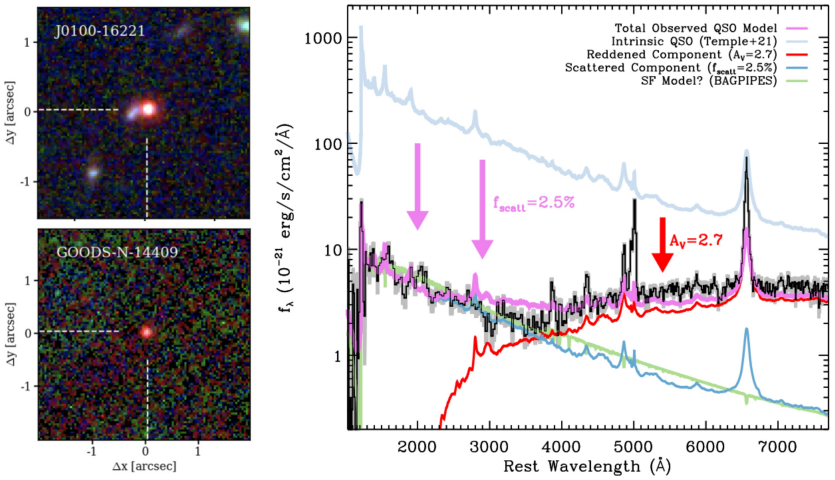

Figure 1.8: *Left:* False-color NIRCam images of two representative "little red dots" (LRDs) from the broad-line AGN sample of Matthee et al. (2024b), showcasing their compact, red morphology. *Right:* Prism/NIRSpec spectrum (black line) of a representative LRD (object MSAID4286), exhibiting the characteristic "V-shaped" spectral energy distribution. The steep red continuum is explained by a heavily reddened AGN template (red line), while the rising UV slope cannot be accounted for by the intrinsic AGN continuum alone. Two alternative components are shown to model the UV excess: (i) scattered AGN light at the ∼2.5% level (light blue), and (ii) moderate star formation from a stellar population model. Figure taken from Greene et al. (2024).

2024), and the underlying seeding and growth pathways of SMBHs in the early Universe (e.g., Li et al. 2024).

A particularly intriguing subset of the JWST AGN candidates – estimated to comprise $\gtrsim 20\%$ of the sample (Harikane et al. 2023; Taylor et al. 2024) – exhibits unusually steep, red continua in the rest-frame optical, along with compact morphologies. These objects have become known as "little red dots" (LRDs). Figure 1.8 presents two representative NIRCam images of such sources from Matthee et al. (2024b), as well as a PRISM/NIRSpec spectrum of an LRD from Greene et al. (2024). The latter illustrates the characteristic "V-shaped" spectral energy distribution (SED), which is created by the combination of a blue component in the rest-frame UV and the rising red continuum in the rest-frame optical. In the pioneering work of Greene et al. (2024), this is interpreted as a combination of a reddened quasar template – accounting for the steeply rising red continuum – and an additional blue component, attributed either to starlight from the host galaxy or to quasar light scattered into our line of sight.

Interestingly, this and other interpretations suggest moderate levels of dust attenuation, typically in the range $A_V \approx 1{-}4$ (Kokorev et al. 2024; Greene et al. 2024). When the SEDs and emission lines of LRDs are corrected

for this extinction, the inferred bolometric luminosities and black hole masses are found to be comparable to those of UV-selected, unobscured quasars identified in pre-JWST surveys (e.g., Fan et al. 2023; Matsuoka et al. 2022). This similarity is striking given the vastly different selection strategies and survey volumes. While UV-luminous quasars at $z \gtrsim 6$ have been discovered in wide-field surveys covering $\sim$ 1400 deg^2 (Matsuoka et al. 2022), the JWST-detected LRDs are emerging from pencil-beam or small fields totaling only $\sim$ 300–600 arcmin^2 (e.g., Matthee et al. 2024b; Kokorev et al. 2024). This implies an apparent overabundance of LRDs by factors of 10^3–10^4, assuming the populations are otherwise comparable – a discrepancy that cannot be easily explained.

This dramatic difference in inferred number densities raises fundamental questions about the nature of LRDs and JWST-selected AGN candidates more broadly. The possibility that they trace a large population of obscured, broad-line quasars that was previously undetected is challenged further by the unusual SED properties of LRDs beyond the rest-frame UV-optical. Multiple studies have reported a set of anomalous features that distinguish LRDs and other JWST AGN candidates from classical quasars, including apparent X-ray weakness (e.g., Yue et al. 2024b), the abundant presence of Balmer absorption features as well as strong Balmer breaks (e.g., Juodžbalis et al. 2024; de Graaff et al. 2025), a potential lack of variability (Kokubo & Harikane 2024), and unexpectedly faint dust emission in both the mid- and far-infrared (e.g., Pérez-González et al. 2024; Casey et al. 2025).

The enigmatic nature of these sources has sparked widespread interest within the community, leading to a steady stream of papers proposing a broad spectrum of theoretical interpretations for the nature of LRDs – ranging from exotic scenarios to more conservative models invoking complex geometries and radiative transfer effects. A simple NASA/ADS search reveals that over ∼150 preprints and peer-reviewed articles in the last two years mention "little red dots" in their title or abstract, underscoring both the scale of engagement and the unsettled nature of this emerging field. While this is not the place to review the full breadth of this rapidly growing literature, the sheer diversity of proposed explanations highlights just how far we remain from a definitive understanding.

Nevertheless, some common themes are beginning to crystallize. Several recent studies suggest that the Balmer absorption features, pronounced Balmer break, and – in some cases – the steep rest-frame optical continua observed in LRDs may arise from dense, cool gas enshrouding a rapidly accreting SMBH (Inayoshi & Maiolino 2025; Naidu et al. 2025) – potentially indicative of super-Eddington accretion flows (e.g., Liu et al. 2025) or even SMBH seeding in the early Universe (e.g., Begelman & Dexter 2025). On the other hand, some studies have questioned whether LRDs host SMBHs at all. In these cases, the broad emission lines – typically seen as signatures of AGN activity – could instead be powered by compact gas in extreme

starburst or rare transient phenomena unrelated to SMBH accretion (e.g., Baggen et al. 2024; Sacchi & Bogdan 2025).

Chapter 4 of this thesis is dedicated to investigating LRDs. Rather than attempting to define what they are, I take a complementary approach – arguing what *they are not*. Using an argument that combines quasar clustering with the observed number density of LRDs, I demonstrate that LRDs cannot merely be obscured counterparts of UV-luminous quasars. The reason is simple: LRDs are too abundant to reside in the same halos where UV-luminous quasars live. Thus, they need to follow intrinsically different scaling relations between SMBHs, host galaxies, and halos than those established for quasars. This conclusion is now supported by emerging clustering measurements, which show that LRDs exhibit spatial correlations consistent with typical field galaxies, in stark contrast to the strong clustering seen in quasars at similar redshifts (Arita et al. 2025; Matthee et al. 2024a; Lin et al. 2025). These results strongly suggest that LRDs are not just dust-obscured versions of the quasars we already know – but instead represent a fundamentally distinct population. They may trace a different evolutionary pathway in SMBH and galaxy growth, or reflect a phase of black hole formation or evolution driven by fundamentally different physical mechanisms. Perhaps they are not accreting SMBHs at all, and could instead reveal something new about extreme stellar processes. Uncovering their true nature remains an exciting and urgent challenge for the field.

1.4 Theoretical models: key uncertainties and future directions

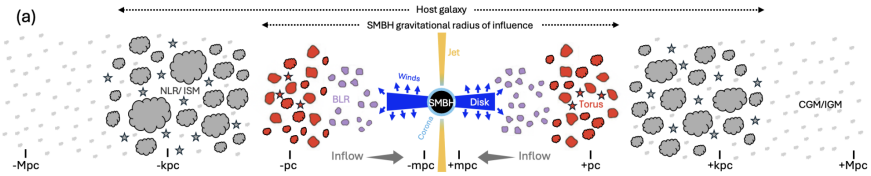

Figure 1.9: Schematic illustration of an AGN (vertical axis is not to scale) embedded within its larger-scale host galaxy and dark matter halo environment, spanning (logarithmic) scales from milli-parsecs to mega-parsecs along the horizontal axis. Key components are marked, including the regions dominated by the SMBH's gravitational influence – the AGN itself: accretion disk, X-ray "corona," possible winds or jets from the disk, broad-line region (BLR), and dusty molecular "torus" – as well as the surrounding host galaxy and halo. Figure adapted from Alexander et al. (2025).

The biggest challenge faced by any first-principles model of SMBH growth in a cosmological context is that of scale. This is illustrated in Figure 1.9, which sketches the vast range of spatial scales involved in SMBH

evolution. Accretion onto SMBHs occurs in a disk that extends from just a few Schwarzschild radii (R_S[3]) out to a few hundred R_S. The AGN central engine also comprises a compact broad-line region (BLR) and a dusty molecular torus – together rarely extending beyond ~ 1 pc. Even so, most of the intrinsic UV-optical/X-ray emission in a type I AGN is confined within the innermost ~ 0.01 pc, a region not much larger than our Solar System.

Although accretion is regulated by processes on the smallest scales, the long-term growth of SMBHs is ultimately driven by galactic and cosmological mechanisms operating across kpc to tens-of-Mpc scales. The enormous energy output from accretion further couples the central AGN regions to the large-scale environment: AGN radiation and feedback can impact structures that are several Mpc away. Reproducing the formation and evolution of SMBHs and quasars in a cosmological framework would thus require resolving both the minuscule scales of accretion and the vast cosmic volumes where such rare objects statistically arise – a task that spans twelve orders of magnitude and will remain computationally unfeasible in the foreseeable future. Even the most advanced zoom-in cosmological hydrodynamical simulations, which focus computational resources on selected halos, typically achieve resolutions no better than ~ 1 pc in the nuclear region[4], and must therefore rely on sub-grid prescriptions to model the unresolved physics of AGN fueling and feedback (Anglés-Alcázar et al. 2021).

Given the extreme range of spatial and physical scales involved, it is perhaps unsurprising that, despite major progress over the past decade in reproducing global galaxy populations and their evolution (see Vogelsberger et al. 2020, for a review), hydrodynamical simulations still struggle to match observational constraints on SMBHs. Most large-scale simulations are calibrated to reproduce local SMBH–galaxy scaling relations – and generally do so with reasonable accuracy (e.g., Di Matteo et al. 2005; Booth & Schaye 2009) – but they diverge widely in their predictions for how SMBHs grow and evolve over cosmic time (Habouzit et al. 2021, 2022; Porras-Valverde et al. 2025). While the sub-grid treatments of star formation – operating on scales of giant molecular clouds, i.e., $\sim 10-100$ pc – are relatively well studied and established, physical models for SMBH growth and AGN feedback remain much more rudimentary and vary substantially across different simulation frameworks.

In recent years, the simulation community has invested considerable effort in refining the treatment of AGN within cosmological simulations, aiming to better connect the physics of SMBH accretion with the broader processes

[3]The Schwarzschild radius of a black hole is given by $R_S = 2M_{BH}/c^2$.

[4]Recent advances now make it possible to resolve the accretion disc of a SMBH within a cosmological simulation by recursively refining the central region (see, e.g., Hopkins et al. 2025). Such simulations, however, can only follow the system over very short timescales, in contrast to standard zoom-in simulations that capture the full cosmological evolution of selected halos.

of galaxy formation and evolution. Notable progress has been made, with important developments proposed in the modeling of black hole seeding (e.g., Bhowmick et al. 2024), dynamics (e.g., Genina et al. 2024), accretion (e.g., Koudmani et al. 2024; Weinberger et al. 2025), and feedback (e.g., Huško et al. 2024). However, despite these advances, significant uncertainties remain, and the predictive power of current simulations for SMBH evolution remains limited.

An alternative to modeling SMBH evolution through first-principles physics is the use of phenomenological or empirical models. These models are agnostic to the detailed physical mechanisms driving black hole growth, instead aiming to capture the observed evolution of SMBHs through simple, parametric formulations that are constrained directly by data. By relying on observations, these models seek to empirically characterize the demographics of SMBHs and their connection to host galaxies in a self-consistent way. While they have limited predictive power beyond the range of the observational constraints they are built upon, they are powerful tools for identifying the key empirical trends that any physical model must reproduce.

Empirical models involving SMBHs can be broadly divided into two main categories. The first class focuses on the evolution of the SMBH mass function by solving the continuity equation. These models rely on two key ingredients: the local observed SMBH masses and the redshift-dependent QLFs. They extend the Soltan (1982) argument to reconstruct the evolution of the SMBH population by linking their growth history to the observed energy output, yielding estimates of key quantities such as the average radiative efficiency, duty cycle, and the distribution of Eddington ratios. Seminal work in this area includes studies by Yu & Tremaine (2002); Merloni & Heinz (2008); Shankar et al. (2009), as well as the more recent models by, e.g., Aversa et al. (2015); Tucci & Volonteri (2017). Collectively, these studies helped to build a statistical picture of SMBH growth across cosmic time.

The second class of models centers on the co-evolution of galaxies and SMBHs, leveraging the empirical relations between galaxy and black hole properties. These models often build upon semi-empirical frameworks originally developed for galaxy evolution, extending them to incorporate SMBHs and AGN activity by assuming a (redshift-dependent) SMBH–galaxy relation. Classic implementations of this approach include Croton (2009), Conroy & White (2013), and Caplar et al. (2015). A notable recent example is TRINITY (Zhang et al. 2023), which extends the halo-galaxy connection formalism of Behroozi et al. (2013) to simultaneously model the evolution of dark matter halos, galaxies, and SMBHs. TRINITY assumes that SMBH growth follows a redshift-evolving relation with galaxy properties and constrains average black hole evolution histories by requiring consistency with a broad range of SMBH and galaxy observables.

Phenomenological models are inherently constrained by the quality and completeness of the observational data they are built upon. In this sense, they reflect the current limits of our ability to probe SMBH evolution. Yet this dependence on data also offers a key strength: as observations improve – particularly at high redshift – these models can be continually refined, allowing for more accurate and insightful reconstructions of black hole growth across cosmic time.

Motivated by the growing body of current and upcoming observations targeting quasars and SMBHs in the early Universe, in Chapter 5 I develop an empirical modeling framework designed to flexibly and self-consistently interpret a wide range of quasar observables. These include luminosity functions, Eddington ratio distributions, and large-scale clustering – including new measurements at high redshift (Sec. 1.3) – all integrated within a unified model built upon a large-volume, dark-matter-only cosmological simulation. By reproducing the diversity of individual black hole growth histories and quasar light curves, this approach enables a systematic exploration of the physical mechanisms that drive SMBH evolution and sheds light on the key processes shaping the high-redshift quasar population.

1.5 This thesis

This thesis presents six studies conducted in collaboration with my co-authors, covering a broad range of topics: the clustering and evolution of high-redshift quasars and supermassive black holes (SMBHs), the emerging population of "little red dots" and JWST-selected AGN candidates, the study of parameter inference for third-generation gravitational wave detectors, and the morphology of protoplanetary discs. While most chapters have already been introduced in earlier sections, I provide below a summary of each chapter – highlighting its objectives and main results – to serve as a reference for navigating the structure of this thesis.

Chapter 2 presents a framework we developed to jointly model the clustering and luminosity function of quasars at arbitrary redshifts. This framework is built on large-volume, dark-matter-only cosmological simulations, and includes a method to extract the relevant halo statistics – i.e., the halo mass function and the cross-correlation of halos with different masses – while combining multiple simulations to increase the dynamic range. With this method, we can effectively probe the largest scales which are needed to find rare, massive halos while retaining the capability of modeling less massive and more common systems.

The primary goal of this chapter is to revisit the quasar clustering measurements reported by Shen et al. (2007), which revealed an unusually strong clustering signal at $z \approx 4$. We demonstrate that reproducing both the quasar luminosity function (QLF) and the clustering amplitude at this

redshift is possible, but only under the extreme assumption that nearly all quasars occupy the most massive dark matter halos. While modeling the QLF or clustering separately admits a wide range of parameter choices, jointly fitting the two observables substantially tightens the constraints – pointing to a quasar duty cycle close to unity and a remarkably small scatter in the luminosity-halo mass relation. These conclusions are both striking and challenging, underscoring the need for new observational campaigns to either confirm or refute the Shen et al. (2007) results. Finally, we highlight the flexibility of our framework by applying it to the quasar clustering measurements at $z \approx 2.5$ from Eftekharzadeh et al. (2015), which provide some of the most precise constraints on quasar clustering currently available.

In **Chapter 3**, we extend the model introduced in Chapter 2 to incorporate the population of line-emitting galaxies observed in JWST WFSS/NIRCam surveys. In particular, we focus on [O III] emitters identified in JWST surveys such as EIGER (Kashino et al. 2023). Capturing both quasars and galaxies within a unified framework requires an exceptionally large cosmological volume, which we achieve using the FLAMINGO-10k dark-matter-only simulation (Schaller et al., in prep.), specifically designed for this purpose. Leveraging this simulation, we successfully reproduce several key observables at $z \approx 6$: the luminosity functions of quasars and [O III] emitters (Schindler et al. 2023; Matthee et al. 2023), their respective auto-correlation functions (Arita et al. 2023; Eilers et al. 2024), and the quasar–galaxy cross-correlation function (Eilers et al. 2024).

The model yields predictions for the luminosity–halo mass relation, host halo mass distributions, and duty cycles for both quasars and [O III] emitters. To our knowledge, this is the first study to constrain the properties of these populations at such high redshifts using clustering measurements. Notably, our results point to a very low quasar duty cycle at $z \approx 6$ ($f_{\rm duty} \lesssim 1\%$). We discuss the implications of these findings for early SMBH and galaxy formation, and highlight the puzzling evolution of quasar properties implied by measurements of quasars clustering at different cosmic epochs.

Chapter 4 investigates a newly emerging population of broad-line AGN candidates identified in deep JWST imaging and spectroscopy – some of which exhibit a steep rest-frame optical continuum and are thus referred to as "little red dots" (LRDs; Matthee et al. 2024b). After correcting for obscuration, many LRDs exhibit bolometric luminosities comparable to UV-selected quasars, despite being detected in surveys covering areas thousands of times smaller (Greene et al. 2024). This striking contrast implies that LRDs are significantly more abundant than unobscured quasars of similar luminosity, posing a major challenge to existing models of SMBH growth and AGN activity in the early Universe (Inayoshi & Ichikawa 2024).

Through a detailed comparison between JWST-selected AGN/LRDs and UV-selected quasars, we conclude that LRDs outnumber quasars by a large and rapidly evolving factor with redshift. Interestingly, this suggests

that the large population of LRDs cannot be accommodated in the same halos where unobscured quasars live, suggesting that LRDs represent a distinct evolutionary phase of SMBH growth, governed by different black hole–galaxy–halo scaling relations. Supporting this interpretation, recent clustering measurements show that LRDs exhibit spatial correlations consistent with typical star-forming galaxies, in stark contrast to the strong clustering seen in quasars at similar redshifts (Arita et al. 2025; Matthee et al. 2024a; Lin et al. 2025). Together, these findings indicate that LRDs are not merely obscured versions of known quasars, but instead constitute a fundamentally distinct population in the early AGN landscape – or possibly, that they are not AGN at all.

Chapter 5 builds on the models developed in Chapters 2 and 3 by introducing an evolutionary framework for SMBHs and quasars embedded within a large dark-matter-only cosmological simulation. As in previous chapters, the model is constrained by key quasar observables – namely, the luminosity function and large-scale clustering – but is now applied consistently across all redshifts within a unified framework. Additionally, SMBH mass measurements (or equivalently, the Eddington ratio distribution function) are incorporated as an independent constraint, in a way that mitigates biases due to the limited completeness of current observations. At its core, the model connects the growth history of each SMBH to that of its host halo through parametric functions that account for both average evolutionary trends and stochastic variability. SMBH growth is treated self-consistently, with accretion directly driving quasar activity.

Despite its simplicity, the model successfully reproduces a broad range of observables from the epoch of reionization ($z \approx 7$) down to cosmic noon ($z \approx 2$). We focus in particular on the early buildup of the most massive SMBHs ($\gtrsim 10^9\,\mathrm{M}_\odot$ by $z \approx 7$), and investigate the primary drivers of this growth – including the relative contributions of accretion and mergers, as well as the role of the accretion coherence timescale. Future extensions of this framework will target lower redshifts and incorporate additional observational constraints, such as quasar proximity zones and damping wing measurements, and the gravitational wave background detected by pulsar timing array (PTA) experiments.

Chapter 6 focuses on parameter inference for gravitational wave (GW) signals in the era of third-generation detectors, such as the Cosmic Explorer (CE; Reitze et al. 2019) and the Einstein Telescope (ET; Punturo et al. 2010). These future observatories will offer unprecedented sensitivity, capable of detecting compact binary coalescences from the earliest epochs of cosmic history. They will routinely observe events with extraordinarily high signal-to-noise ratios (SNRs) reaching several thousand. This leap in sensitivity – along with a redshift reach an order of magnitude beyond current detectors – will open new windows into precision cosmology, tests of gravity, and astrophysical models of binary formation and evolution (Abac et al. 2025).

However, with this increased detection capability come new challenges. One of the most pressing is the overlap of multiple GW signals in the time domain due to the high event rate (Baibhav et al. 2019). When signals overlap in time or frequency, standard data analysis pipelines may no longer be reliable, potentially introducing significant biases in the inferred source parameters.

In our exploratory study, we were among the first (see also the independent analysis by Samajdar et al. 2021) to quantify these biases by testing existing parameter inference pipelines in the presence of overlapping GW signals. We simulate various configurations of two overlapping signals from non-spinning binaries, systematically varying their relative SNRs, coalescence times, and merger phases. We show that – by setting a prior on the coalescence time using the information from detection pipelines, which are typically accurate to within ~ 10 ms (Regimbau et al. 2012; Meacher et al. 2016) – it is possible to correctly infer the properties of multiple overlapping signals even with the current data-analysis infrastructure, provided that the coalescence times of the signals in the detector frame are more than $\sim 1-2$ seconds apart. However, if the coalescence times differ by less than ~ 0.5 seconds, significant biases arise, highlighting the need for new analysis strategies and algorithms (e.g., Baka et al. 2025).

Chapter 7 shifts focus to the physics of protoplanetary discs. As in the case of accretion discs around SMBHs, gas turbulence plays a central role in driving accretion and the secular evolution of protoplanetary discs. However, in this context, its influence extends well beyond accretion alone – it affects a wide range of processes that are crucial for planet formation. Quantifying the level of gas turbulence in discs is therefore one of the key open questions in the field (Rosotti 2023).

A promising approach to constraining turbulence is to measure the vertical scale height of the dust layer in discs, which is expected to trace the gas structure through gas–dust coupling. This has become feasible thanks to the unprecedented resolution of ALMA observations, which have revealed detailed substructures – such as rings and gaps – in the 2D emission profiles of protoplanetary discs (Bae et al. 2022). As shown by Pinte et al. (2016), it is possible to exploit these features to uncover the 3D morphology of discs. The idea is simple: due to projection effects, a gap in a disc's emission profile will be partly filled by the emission coming from the neighbouring regions. This effect is stronger along the minor axis of the disc, whereas the major axis is only marginally affected. Hence, one can compare the gap contrast along the major and minor axes to infer the degree of this "filling", which in turn depends on the disc's vertical thickness.

In our study, we applied this technique to high-resolution ALMA data from the DSHARP survey (Andrews et al. 2018), constructing radiative transfer models to reproduce the observed gap contrast for varying dust scale heights. We find that, in discs where constraints are possible, the preferred models favor small scale heights, indicating low levels of gas turbulence. For

the remaining nine systems in our sample, our method yields no meaningful constraints, likely due to either low disc inclination or insufficiently deep gaps. Based on our analysis, we propose an empirical criterion to assess whether a given disc is suitable for this technique, offering a valuable tool for guiding future observational efforts.

Bibliography

Abac A., et al., 2025, arXiv e-prints, p. arXiv:2503.12263
Abbott B. P., et al., 2016, Phys. Rev. Lett., 116, 061102
Abbott B. P., et al., 2019, Physical Review X, 9, 031040
Abbott R., et al., 2023, Physical Review X, 13, 011048
Agazie G., et al., 2023, ApJ, 951, L8
Aird J., et al., 2015, ApJ, 815, 66
Akiyama M., et al., 2018, PASJ, 70, S34
Alexander D. M., et al., 2025, arXiv e-prints, p. arXiv:2506.19166
Amaro-Seoane P., et al., 2023, Living Reviews in Relativity, 26, 2
Andrews S. M., et al., 2018, ApJ, 869, L41
Anglés-Alcázar D., Özel F., Davé R., Katz N., Kollmeier J. A., Oppenheimer B. D., 2015, ApJ, 800, 127
Anglés-Alcázar D., et al., 2021, ApJ, 917, 53
Angulo R. E., Hahn O., 2022, Living Reviews in Computational Astrophysics, 8, 1
Arita J., et al., 2023, ApJ, 954, 210
Arita J., Kashikawa N., Onoue M., Yoshioka T., Takeda Y., Hoshi H., Shimizu S., 2025, MNRAS, 536, 3677
Asgari M., Mead A. J., Heymans C., 2023, The Open Journal of Astrophysics, 6, 39
Aversa R., Lapi A., de Zotti G., Shankar F., Danese L., 2015, ApJ, 810, 74
Bae J., Isella A., Zhu Z., Martin R., Okuzumi S., Suriano S., 2022, arXiv e-prints, p. arXiv:2210.13314
Baggen J. F. W., et al., 2024, ApJ, 977, L13
Baibhav V., Berti E., Gerosa D., Mapelli M., Giacobbo N., Bouffanais Y., Di Carlo U. N., 2019, Phys. Rev. D, 100, 064060
Baka T., Narola H., Janquart J., Samajdar A., Dietrich T., Van Den Broeck C., 2025, arXiv e-prints, p. arXiv:2507.10304
Balick B., Brown R. L., 1974, ApJ, 194, 265
Barkana R., Loeb A., 2001, Phys. Rep., 349, 125
Baron D., Ménard B., 2019, Monthly Notices of the Royal Astronomical Society, 484, 5017
Begelman M. C., Dexter J., 2025, arXiv e-prints, p. arXiv:2507.09085
Behroozi P. S., Wechsler R. H., Conroy C., 2013, ApJ, 770, 57
Bhowmick A. K., Blecha L., Torrey P., Weinberger R., Kelley L. Z., Vogelsberger M., Hernquist L., Somerville R. S., 2024, MNRAS, 529, 3768
Bocquet S., Saro A., Dolag K., Mohr J. J., 2016, MNRAS, 456, 2361
Bogdán Á., Lovisari L., Volonteri M., Dubois Y., 2018, ApJ, 852, 131
Bogdán Á., et al., 2024, Nature Astronomy, 8, 126
Bolton C. T., 1972, Nature, 235, 271

Bond J. R., Kofman L., Pogosyan D., 1996, Nature, 380, 603
Booth C. M., Schaye J., 2009, MNRAS, 398, 53
Bower R. G., Benson A. J., Malbon R., Helly J. C., Frenk C. S., Baugh C. M., Cole S., Lacey C. G., 2006, MNRAS, 370, 645
Boyle B. J., Shanks T., Croom S. M., Smith R. J., Miller L., Loaring N., Heymans C., 2000, MNRAS, 317, 1014
Bromm V., Loeb A., 2003, The Astrophysical Journal, 596, 34
Buchner J., et al., 2015, ApJ, 802, 89
Burke-Spolaor S., et al., 2019, A&A Rev., 27, 5
Caplar N., Lilly S. J., Trakhtenbrot B., 2015, ApJ, 811, 148
Carniani S., et al., 2024, Nature, 633, 318
Casey C. M., et al., 2025, arXiv e-prints, p. arXiv:2505.18873
Chen H., et al., 2022, ApJ, 931, 29
Ciotti L., Haiman Z., Ostriker J. P., 2003, in Bender R., Renzini A., eds, The Mass of Galaxies at Low and High Redshift. p. 106 (arXiv:astro-ph/0112131), doi:10.1007/10899892_25
Conroy C., White M., 2013, ApJ, 762, 70
Cooray A., Sheth R., 2002, Phys. Rep., 372, 1
Crain R. A., van de Voort F., 2023, ARA&A, 61, 473
Croom S. M., Smith R. J., Boyle B. J., Shanks T., Miller L., Outram P. J., Loaring N. S., 2004, MNRAS, 349, 1397
Croom S. M., et al., 2005, MNRAS, 356, 415
Croton D. J., 2009, MNRAS, 394, 1109
Croton D. J., et al., 2006, MNRAS, 365, 11
Davies F. B., Hennawi J. F., Eilers A.-C., 2019, ApJ, 884, L19
Davis M., Efstathiou G., Frenk C. S., White S. D. M., 1985, Astrophysical Journal, 292, 371
Davis B. L., Graham A. W., Cameron E., 2019, Astrophysical Journal, 873, 85
Dawson K. S., et al., 2013, The Astronomical Journal, 145, 10
Dawson K. S., et al., 2016, The Astronomical Journal, 151, 44
Dayal P., Ferrara A., 2018, Phys. Rep., 780, 1
Dayal P., et al., 2024, arXiv e-prints, p. arXiv:2401.11242
Devecchi B., Volonteri M., 2009, ApJ, 694, 302
Di Matteo T., Springel V., Hernquist L., 2005, Nature, 433, 604
Ding X., et al., 2023, Nature, 621, 51
EPTA Collaboration et al., 2023, A&A, 678, A50
Eckart A., Genzel R., 1996, Nature, 383, 415
Efstathiou G., Davis M., Frenk C. S., White S. D. M., 1985, Astrophysical Journal Supplement Series, 57, 241
Eftekharzadeh S., et al., 2015, MNRAS, 453, 2779
Eilers A.-C., Hennawi J. F., Davies F. B., Simcoe R. A., 2021, ApJ, 917, 38
Eilers A.-C., et al., 2024, arXiv e-prints, p. arXiv:2403.07986
Event Horizon Telescope Collaboration et al., 2019, ApJ, 875, L1

Event Horizon Telescope Collaboration et al., 2022, ApJ, 930, L12
Fabian A. C., 2012, ARA&A, 50, 455
Fan X., Bañados E., Simcoe R. A., 2023, ARA&A, 61, 373
Ferrarese L., Merritt D., 2000, Astrophysical Journal Letters, 539, L9
Forouhar Moreno V. J., Helly J., McGibbon R., Schaye J., Schaller M., Han J., Kugel R., 2025, arXiv e-prints, p. arXiv:2502.06932
Friedmann A., 1922, Zeitschrift für Physik, 10, 377
Friedmann A., 1924, Zeitschrift für Physik, 21, 326
Gebhardt K., et al., 2000, Astrophysical Journal Letters, 539, L13
Genina A., Springel V., Rantala A., 2024, MNRAS, 534, 957
Ghez A. M., et al., 2008, The Astrophysical Journal, 689, 1044
Greene J. E., Strader J., Ho L. C., 2020, Annual Review of Astronomy and Astrophysics, 58, 257
Greene J. E., et al., 2024, ApJ, 964, 39
Häberle M., et al., 2024, Nature, 631, 285
Habouzit M., et al., 2021, MNRAS, 503, 1940
Habouzit M., et al., 2022, MNRAS, 509, 3015
Haiman Z., Hui L., 2001, ApJ, 547, 27
Haiman Z., Loeb A., 2001, ApJ, 552, 459
Harikane Y., et al., 2023, ApJ, 959, 39
Heckman T. M., Best P. N., 2014, ARA&A, 52, 589
Heger A., Fryer C. L., Woosley S. E., Langer N., Hartmann D. H., 2003, The Astrophysical Journal, 591, 288
Hellings R. W., Downs G. S., 1983, ApJ, 265, L39
Hopkins P. F., Hernquist L., Cox T. J., Di Matteo T., Robertson B., Springel V., 2006, ApJS, 163, 1
Hopkins P. F., Richards G. T., Hernquist L., 2007, ApJ, 654, 731
Hopkins P. F., et al., 2025, The Open Journal of Astrophysics, 8, 48
Hubble E., 1925, Popular Astronomy, 33, 252
Hubble E. P., 1929, Proceedings of the National Academy of Sciences, 15, 168
Huško F., Lacey C. G., Schaye J., Nobels F. S. J., Schaller M., 2024, MNRAS, 527, 5988
Inayoshi K., Ichikawa K., 2024, ApJ, 973, L49
Inayoshi K., Maiolino R., 2025, ApJ, 980, L27
Inayoshi K., Visbal E., Haiman Z., 2020, ARA&A, 58, 27
Juodžbalis I., et al., 2024, MNRAS, 535, 853
Kashino D., Lilly S. J., Matthee J., Eilers A.-C., Mackenzie R., Bordoloi R., Simcoe R. A., 2023, ApJ, 950, 66
Kim S., et al., 2009, ApJ, 695, 809
Kocevski D. D., et al., 2023, ApJ, 954, L4
Kocevski D. D., et al., 2024, arXiv e-prints, p. arXiv:2404.03576
Kokorev V., et al., 2024, ApJ, 968, 38
Kokubo M., Harikane Y., 2024, arXiv e-prints, p. arXiv:2407.04777

Kormendy J., 1988, ApJ, 335, 40
Kormendy J., Ho L. C., 2013, ARA&A, 51, 511
Koudmani S., Somerville R. S., Sijacki D., Bourne M. A., Jiang Y.-F., Profit K., 2024, MNRAS, 532, 60
Kulkarni G., Worseck G., Hennawi J. F., 2019, MNRAS, 488, 1035
Lambrides E., et al., 2024, arXiv e-prints, p. arXiv:2409.13047
Lapi A., Shankar F., Bosi M., Roberts D., Fu H., Varadarajan K. M., Boco L., 2025, arXiv e-prints, p. arXiv:2507.15436
Larson R. L., et al., 2023, ApJ, 953, L29
Latif M. A., Ferrara A., 2016, PASA, 33, e051
Lemaître G., 1931, MNRAS, 91, 483
Li W., et al., 2024, ApJ, 969, 69
Li J., et al., 2025, ApJ, 981, 19
Lin X., et al., 2025, arXiv e-prints, p. arXiv:2505.02896
Liu H., Jiang Y.-F., Quataert E., Greene J. E., Ma Y., 2025, arXiv e-prints, p. arXiv:2507.07190
Lupi A., Haiman Z., Volonteri M., 2021, MNRAS, 503, 5046
Lynden-Bell D., 1969, Nature, 223, 690
Lynden-Bell D., Rees M. J., 1971, MNRAS, 152, 461
Madau P., Giallongo E., Grazian A., Haardt F., 2024, ApJ, 971, 75
Magorrian J., et al., 1998, Astronomical Journal, 115, 2285
Maiolino R., et al., 2024, A&A, 691, A145
Marshall M. A., et al., 2023, A&A, 678, A191
Martini P., Weinberg D. H., 2001, ApJ, 547, 12
Matsuoka Y., et al., 2022, ApJS, 259, 18
Matthee J., Mackenzie R., Simcoe R. A., Kashino D., Lilly S. J., Bordoloi R., Eilers A.-C., 2023, ApJ, 950, 67
Matthee J., et al., 2024a, arXiv e-prints, p. arXiv:2412.02846
Matthee J., et al., 2024b, ApJ, 963, 129
Meacher D., Cannon K., Hanna C., Regimbau T., Sathyaprakash B. S., 2016, Phys. Rev. D, 93, 024018
Mead A. J., Verde L., 2021, MNRAS, 503, 3095
Merloni A., Heinz S., 2008, MNRAS, 388, 1011
Mo H. J., White S. D. M., 1996, MNRAS, 282, 347
Naidu R. P., et al., 2025, arXiv e-prints, p. arXiv:2503.16596
Nelson D., et al., 2019, Computational Astrophysics and Cosmology, 6, 2
Novak G. S., Ostriker J. P., Ciotti L., 2011, ApJ, 737, 26
Omukai K., Schneider R., Haiman Z., 2008, The Astrophysical Journal, 686, 801
Onions J., et al., 2012, MNRAS, 423, 1200
Ono Y., et al., 2023, ApJ, 951, 72
Pacucci F., Loeb A., 2020, ApJ, 895, 95
Pacucci F., Loeb A., 2022, MNRAS, 509, 1885
Pacucci F., Narayan R., 2024, ApJ, 976, 96

Pacucci F., Nguyen B., Carniani S., Maiolino R., Fan X., 2023, ApJ, 957, L3
Padovani P., et al., 2017, A&A Rev., 25, 2
Peebles P. J. E., 1980, The large-scale structure of the universe
Pérez-González P. G., et al., 2024, ApJ, 968, 4
Pinte C., Dent W. R. F., Ménard F., Hales A., Hill T., Cortes P., de Gregorio-Monsalvo I., 2016, ApJ, 816, 25
Pizzati E., Hennawi J. F., Schaye J., Schaller M., 2024, MNRAS, 528, 4466
Pizzati E., Hennawi J. F., Schaye J., Eilers A.-C., Huang J., Schindler J.-T., Wang F., 2025, MNRAS, 539, 2910
Planck Collaboration et al., 2014, A&A, 571, A1
Porciani C., Norberg P., 2006, MNRAS, 371, 1824
Porciani C., Magliocchetti M., Norberg P., 2004, MNRAS, 355, 1010
Porras-Valverde A. J., Ricarte A., Natarajan P., Somerville R. S., Gabrielpillai A., Yung L. Y. A., 2025, arXiv e-prints, p. arXiv:2504.11566
Press W. H., Schechter P., 1974, ApJ, 187, 425
Punturo M., et al., 2010, Class. Quant. Grav., 27, 194002
Quadri G., Trinca A., Lupi A., Colpi M., Volonteri M., 2025, arXiv e-prints, p. arXiv:2505.05556
Reardon D. J., et al., 2023, ApJ, 951, L6
Regimbau T., et al., 2012, Phys. Rev. D, 86, 122001
Reines A. E., Volonteri M., 2015, ApJ, 813, 82
Reitze D., et al., 2019, in Bulletin of the American Astronomical Society. p. 35 (arXiv:1907.04833)
Richards G. T., et al., 2006, AJ, 131, 2766
Rosotti G. P., 2023, New Astronomy Reviews, 96, 101674
Ross N. P., et al., 2009, ApJ, 697, 1634
Ross N. P., et al., 2013, ApJ, 773, 14
Sacchi A., Bogdan A., 2025, arXiv e-prints, p. arXiv:2505.09669
Salpeter E. E., 1964, ApJ, 140, 796
Samajdar A., Janquart J., Van Den Broeck C., Dietrich T., 2021, Phys. Rev. D, 104, 044003
Sargent W. L. W., Young P. J., Boksenberg A., Shortridge K., Lynds C. R., 1978, The Astrophysical Journal, 221, 731
Sazonov S. Y., Ostriker J. P., Ciotti L., Sunyaev R. A., 2005, MNRAS, 358, 168
Schaye J., et al., 2015, Monthly Notices of the Royal Astronomical Society, 446, 521
Schindler J.-T., et al., 2023, ApJ, 943, 67
Schmidt M., 1963, Nature, 197, 1040
Sesana A., Volonteri M., Haardt F., 2007, MNRAS, 377, 1711
Shankar F., Weinberg D. H., Miralda-Escudé J., 2009, ApJ, 690, 20
Shankar F., Crocce M., Miralda-Escudé J., Fosalba P., Weinberg D. H., 2010, ApJ, 718, 231
Shen Y., et al., 2007, AJ, 133, 2222

Shen X., Hopkins P. F., Faucher-Giguère C.-A., Alexander D. M., Richards G. T., Ross N. P., Hickox R. C., 2020, MNRAS, 495, 3252
Sijacki D., Springel V., Di Matteo T., Hernquist L., 2007, MNRAS, 380, 877
Simpson C., Mortlock D., Warren S., Cantalupo S., Hewett P., McLure R., McMahon R., Venemans B., 2014, MNRAS, 442, 3454
Sądowski A., Narayan R., McKinney J. C., Tchekhovskoy A., 2014, MNRAS, 439, 503
Soltan A., 1982, MNRAS, 200, 115
Somerville R. S., Davé R., 2015, ARA&A, 53, 51
Spergel D. N., et al., 2007, ApJS, 170, 377
Stone M. A., Lyu J., Rieke G. H., Alberts S., Hainline K. N., 2023, arXiv e-prints, p. arXiv:2310.18395
Tanaka T., Haiman Z., 2009, ApJ, 696, 1798
Taylor A. J., et al., 2024, arXiv e-prints, p. arXiv:2409.06772
The LIGO Scientific Collaboration the Virgo Collaboration the KAGRA Collaboration 2025, arXiv e-prints, p. arXiv:2507.08219
Tinker J., Kravtsov A. V., Klypin A., Abazajian K., Warren M., Yepes G., Gottlöber S., Holz D. E., 2008, ApJ, 688, 709
Trimble V., 1995, Publications of the Astronomical Society of the Pacific, 107, 1133
Trinca A., et al., 2024, arXiv e-prints, p. arXiv:2412.14248
Tucci M., Volonteri M., 2017, A&A, 600, A64
Übler H., et al., 2023, arXiv e-prints, p. arXiv:2312.03589
Ueda Y., Akiyama M., Hasinger G., Miyaji T., Watson M. G., 2014, ApJ, 786, 104
Vogelsberger M., et al., 2014, MNRAS, 444, 1518
Vogelsberger M., Marinacci F., Torrey P., Puchwein E., 2020, Nature Reviews Physics, 2, 42
Volonteri M., Rees M. J., 2006, ApJ, 650, 669
Volonteri M., Haardt F., Madau P., 2003, ApJ, 582, 559
Volonteri M., Lodato G., Natarajan P., 2008, MNRAS, 383, 1079
Volonteri M., Silk J., Dubus G., 2015, ApJ, 804, 148
Volonteri M., Habouzit M., Colpi M., 2021, Nature Reviews Physics, 3, 732
Wang F., et al., 2021, ApJ, 907, L1
Wang B. Y., Zhou Y., Chen W., Chen N., Di Matteo T., Croft R., Bird S., Ni Y., 2025, arXiv e-prints, p. arXiv:2503.24304
Weinberger R., Bhowmick A., Blecha L., Bryan G., Buchner J., Hernquist L., Hlavacek-Larrondo J., Springel V., 2025, arXiv e-prints, p. arXiv:2502.13241
White M., Martini P., Cohn J. D., 2008, MNRAS, 390, 1179
White M., et al., 2012, MNRAS, 424, 933
Wolfe A. M., Burbidge G. R., 1970, ApJ, 161, 419
Wu Q., Shen Y., 2022, ApJS, 263, 42
Wu J., et al., 2022, MNRAS, 517, 2659

Wyithe J. S. B., Loeb A., 2009, MNRAS, 395, 1607
Xu H., et al., 2023, Research in Astronomy and Astrophysics, 23, 075024
York D. G., et al., 2000, AJ, 120, 1579
Yu Q., Tremaine S., 2002, MNRAS, 335, 965
Yue M., et al., 2024a, ApJ, 966, 176
Yue M., Eilers A.-C., Ananna T. T., Panagiotou C., Kara E., Miyaji T., 2024b, ApJ, 974, L26
Zel'dovich Y. B., Novikov I. D., 1967, Soviet Astronomy, 10, 602
Zhang H., Behroozi P., Volonteri M., Silk J., Fan X., Hopkins P. F., Yang J., Aird J., 2023, MNRAS, 518, 2123
Zhang W., Shu X., Sun L., Shen R.-F., Dou L., Jiang N., Wang T., 2025, Nature Astronomy, 9, 702
Zou F., Brandt W. N., Gallo E., Luo B., Ni Q., Xue Y., Yu Z., 2024, ApJ, 976, 6
da Ângela J., et al., 2008, MNRAS, 383, 565
de Graaff A., et al., 2025, arXiv e-prints, p. arXiv:2503.16600
Ďurovčíková D., et al., 2024, ApJ, 969, 162